QUANTUM IMAGING AND SENSING WITH ENTANGLED

PHOTONS

By

AZIZ KOLKIRAN

Bachelor of Science in Physics
Middle East Technical University
Ankara, Turkey
1996

Master of Science in Physics
Middle East Technical University
Ankara, Turkey
1999

Submitted to the Faculty of the
Graduate College of
Oklahoma State University
in partial fulfillment of
the requirements for
the Degree of
DOCTOR OF PHILOSOPHY
July, 2008

QUANTUM IMAGING AND SENSING WITH ENTANGLED PHOTONS

Dissertation Approved:

Dr. Girish S. Agarwal
_____
Dissertation Advisor

Dr. Jacques H. H. Perk
_____

Dr. Gil Summy
_____

Dr. Alan Cheville
_____

Dr. A. Gordon Emslie
_____
Dean of the Graduate College

ACKNOWLEDGMENTS

I am indebted to my advisor, Prof. Girish S. Agarwal, for his guidance and support throughout the course of my work leading to this dissertation. His rich knowledge, insight and a deep understanding of physics, and more importantly the way he explores highest quality problems will remain exemplary for me wherever I will go. It has been a special privilege for me to be in his group, as the work was led in a very open and motivating way, allowing me to include my personal ideas and approach in this research.

Many thanks are also due to Prof. Jacques H. H. Perk for his help with the preparation of this thesis. My appreciation extends to my other committee members Prof. Gil Summy and Prof. Alan Cheville, whose comments have also been invaluable.

I also would like to express my sincere appreciation to Prof. Paul Westhaus and Prof. James P. Wicksted for their assistance and support during these years of my study at Oklahoma State University.

I am grateful to office staff members Susan Cantrell, Cindi Raymond, Stephanie Hall and Danyelle Talbot for their continuous help in various ways.

Finally, I wish to express my love and gratitude to my beloved mother, Emine Kolkıran. This work and all the achievements in my life would have been impossible without the endless support, patience and understanding of my mother. She did everything she could in order to provide me with the best possible education. I always felt her love and affection at the highest order wherever I went for my studies. She is always in my heart, my thoughts and prayers. I thank God everyday for blessing me with such a wonderful mother.

TABLE OF CONTENTS

viii

CHAPTER 1

INTRODUCTION

Quantum imaging is a newly born branch of quantum optics that investigates the ultimate performance limits of optical imaging allowed by the laws of quantum mechanics. Using the methods and techniques from quantum optics, quantum imaging addresses the questions of image formation, processing and detection with sensitivity and resolution exceeding the limits of classical imaging. Particularly, the manipulation of quantum entanglement has found enormous potential for improving performances in the techniques of quantum imaging such as quantum interferometry, lithography, microscopy and geometrical optics. Similar improvements have led to new types of high-precision measurement, which can be grouped under quantum sensing or quantum metrology. In this chapter, we give a brief introduction and survey to the systems and technologies of quantum imaging and sensing.

1.1 QUANTUM IMAGING AND SENSING SYSTEMS

1.1.1 Quantum interferometry

Interferometry is one of the most fundamental and widely used methods to detect the interference between two or more waves. In addition to its fundamental scientific importance, interferometry is widely used in all kinds of optical imaging and sensing applications. On the other hand, the concept of quantum interference gives a deeper and more general understanding of the interference phenomena in physics. It demonstrates the wave nature of massive particles more than anything else. The impact of quantum interference on light experiments is associated with the quantization of the

field where the energy of a light mode is quantized to be multiples of a basic unit, the photon energy. For light, the quantum effects become apparent, for example, when performing experiments with single photons. When one is dealing with such particles, interferometry cannot be described by the superposition of waves, as in classical optics, and a different description of interferometry is required. Therefore, we need a quantum interference method which is capable of utilizing the states of light that can only be described in a quantized fashion. Quantum interferometry is the field of quantum optics implementing the quantum interference phenomena utilizing states which can be described only in a quantum mechanical way.
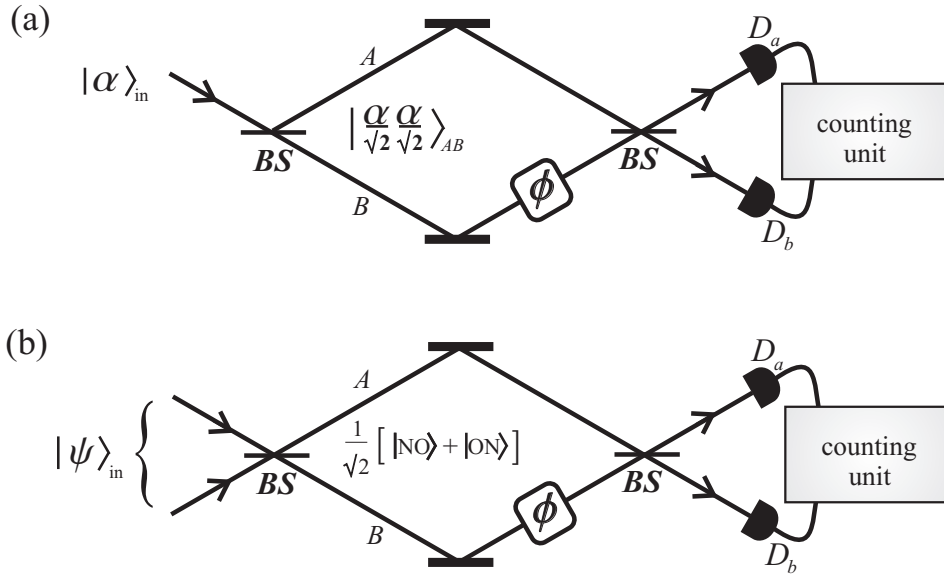
Figure 1.1: The optical interferometer by using (a) one-port coherent source $|\alpha\rangle_{in}$, and (b) two-port correlated source. In (b), the path entangled N-photon state $(\frac{1}{\sqrt{2}}[|N0\rangle_{AB} + |0N\rangle_{AB}])$ between the two beam splitters (BS) is a superposition of N photons altogether being in mode A or in mode B. For $N = 2$, the input state $|\psi\rangle_{in}$ would be $|11\rangle_{in}$.

In a conventional optical interferometer (see Fig. 1.1(a)), in which light in a co-

herent state enters via only one port, the minimum phase sensitivity, $\Delta\phi$, scales as $1/\sqrt{N}$, where N is the number of photons passing through the interferometer per unit time. However, if carefully prepared quantum correlations are engineered between the photons entering through the two input ports (see Fig. 1.1(b)), then the interferometer sensitivity improves by a factor of $\sqrt{N}$, to scale like $1/N$, which is the limit imposed by the Heisenberg Uncertainty Principle. This favorable scaling with N means that, for large numbers of photons, a dramatic improvement in measurement sensitivity should be possible. This may be of great importance in a number of areas of physics including, for example, the detection of gravitational waves. In addition to the increased phase measurement precision, quantum correlated photons can increase the resolution of the interference pattern by using a special detection scheme. This super-resolution increases the image quality by increasing the number of distinguishable bright points or number of pixels per unit area. This is classically limited by the wavelength of the light source. In quantum interferometry, by using N quantum entangled photons at a time, the number of pixels can be increased N^2-times that of uncorrelated ones.

1.1.2 Quantum interferometric lithography and microscopy

The classical resolution limit was established by Rayleigh at the end of the nineteenth century and it states that the resolution in an optical system is limited by diffraction on its optical elements due to the wave nature of light. According to this criterion, two closely spaced points at the input of the optical system cannot be resolved if the distance between them is smaller than $\lambda/4$ where λ is the wavelength of the light. In optical-lithographic semiconductor etching techniques, the Rayleigh diffraction limit puts a lower bound on the feature size that can be printed on chip. It is, in principle, possible to work with shorter wavelengths. However, such an approach introduces other problems. The optical elements working in the UV and X-ray regions of the

spectrum is technologically and commercially difficult to produce and the problems become worse the shorter you go. Therefore, at this point, one may ask the question of how to beat the limit set by the Rayleigh criterion. Recent developments in the quantum imaging techniques has shown that the limit of resolution also depends on the strong non-local correlation properties of the light used to image the system. It has been shown that the classical diffraction limit in lithography can be circumvented by the use of path-entangled photon number states [1]. If N photons are path-entangled in a special superposition state, $[|N0\rangle + |0N\rangle]/\sqrt{2}$ (also known as $NOON$ state, see Fig. 1.1(b)), and if the recording medium responds by N-photon absorption, features of size $\lambda/4N$ can be written into the material. That is, the geometric distance between the two points that can be distinguished according to the Rayleigh limit is now N times smaller than the classical case. As a consequence, we can in principle read and write much smaller features with this technique. The proof-of-principle experiments displaying various aspects of this technique have been reported [2, 3].

1.1.3 Quantum metrology and precision measurements

Quantum metrology is the study of making high-resolution (super-resolution) and highly sensitive (super-sensitivity) measurements of physical parameters using quantum theory to describe the physical systems, particularly exploiting quantum entanglement [4]. It promises to develop measurement techniques that give better precision than the same measurement performed in a classical framework. Many precision measurements can be reformulated in terms of a phase measurement. For example, one can send light through a medium with an unknown index of refraction n to induce a phase shift $\phi = 2\pi L(n - 1)/\lambda$, with λ the wavelength of the light and L the length of the medium. This phase shift can be measured relative to a reference beam in a Mach-Zehnder interferometer. When L and λ are known with very high precision, one can infer the index of refraction with an accuracy that is proportional to the

4

error in phase. The next question is, how well one can measure ϕ given a quantum state $|\psi(\phi)\rangle$ which has the phase ϕ as a dynamical parameter. That is, we want an expression for the error, $\Delta\phi$, in the phase. For a coherent state input having N photons on average, one can reach an optimum accuracy of $\Delta\phi = 1/\sqrt{N}$, which is the standard quantum limit or shot noise limit. However, it is found that this limit is not fundamental and the sensitivity of phase measurement depends on the nonclassical correlation properties of the input state. For example, if N photons are utilized in a $NOON$ state superposition, by choosing a suitable measurement operator, one can obtain a phase measurement accuracy of $\Delta\phi = 1/N$. This phase sensitivity, which is inversely proportional to the total number of photons involved, is known as the Heisenberg limit and it is proven to be the fundamental (unsurpassable) quantum limit for the phase measurement [5]. This $\sqrt{N}$ precision enhancement of the entangled sources over the classical ones is related to the fact that the entangled states can evolve faster than the unentangled configurations employing the same sources [6]. Quantum metrology is not unique to photonic states, it can be realized in any physical system that can be described in a quantum mechanical fashion.

1.1.4 Quantum non-distortion interrogation and ghost imaging

Quantum imaging has led to some other important breakthroughs as well, such as the possibility of imaging without interaction (non-distortion interrogation) and reproducing "ghost" images in a non-local manner: In non-interactive quantum imaging (sensing), using single photons in an interferometric setting, it is possible to image or detect an object, without a photon actually interacting with the object. Hence, one can see what something looks like, without shining any light on it. This result has been born out in a series of experiments by P. Kwiat and A. Zeilinger [7, 8]. On the other hand, in ghost imaging, the idea is to make use of entangled photons to form an image of an inaccessible object. One of the two entangled beams of light illuminates

the object. The other beam, by a correlation measurement, produces the image non-locally without interacting with the object. The phenomenon of ghost imaging was first demonstrated experimentally by Pittman *et al.* in 1995 [9]. Since then, the field has evolved to the point of the development of practical applications which exploit the greater resolution and nonlocal behavior of ghost imaging. Currently, there is an intense technological and experimental effort to bring these breakthrough ideas of quantum imaging into practicality for realistic problems.

1.2   PARAMETRIC DOWN CONVERSION AS A SOURCE OF QUANTUM IMAGING AND SENSING

The process of spontaneous parametric down conversion (SPDC) has been a work horse for the last two decades in understanding a variety of issues in quantum physics and in applications in the field of quantum imaging [10, 11, 12, 13, 14]. It is a process that is used to produce light possessing strong quantum features. Photon pairs generated by this process show entanglement with respect to different physical attributes such as time of arrival and states of polarization [14, 15]. They are increasingly being utilized for very basic experiments to test the foundations of quantum mechanics and to do quantum information processing [14, 16]. It is also recognized that entangled photon pairs could be useful in many practical applications in precision metrology involving, e.g., interferometry [17, 18, 19, 20], imaging [9, 21], lithography [1, 2, 22, 23], and spectroscopy [24].

Roughly speaking, down conversion is the conversion of a pump photon into signal and idler photons within a nonlinear medium. Crystals of a certain chemical structure, such as BBO (Beta Barium Borate), LBO (Lithium Barium Borate), or KDP (Dihydrogen Phosphate), have the property of optical nonlinearity, which means that the polarizability of these crystals depends on the square (or higher powers) of an applied electric field. The practical outcome of this property is that, when passing through
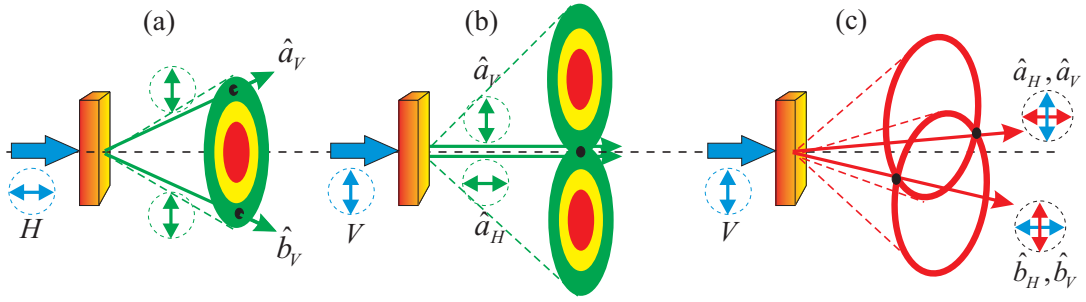
Figure 1.2: Parametric down-conversion with different phase matching conditions. (a) Type-I non-collinear geometry, (b) Type-II collinear geometry and (c) Type-II non-collinear geometry.

such a crystal, a single-parent photon splits (down-converts) into a pair of daughter photons (signal and idler). The probability that this event occurs is extremely small; on average, it happens to only one out of every 10 billion photons. When the down-conversion does occur, energy and momentum are conserved (equivalently known as the frequency and phase-matching conditions):

$$\omega_p = \omega_s + \omega_i, \qquad \mathbf{k}_p = \mathbf{k}_s + \mathbf{k}_i, \tag{1.1}$$

where $\omega_j, \mathbf{k}_j$ $(j = s, i, p)$ are the frequency and wavevector of the signal (s), idler (i), and pump (p) photons. The daughter photons have lower frequencies than the parent photon and emerge from the crystal on opposite sides of a cone that is centered about the direction traveled by the parent. In Type-I phase matching the daughters emerge from a specifically oriented crystal with identical polarizations that are aligned perpendicular to the parent polarization—see Fig. 1.2(a). For the case when the signal and idler photons have orthogonal polarizations (one "H" and one "V"), then the down-conversion is Type-II—see Fig. 1.2(b) and Fig. 1.2(c).

The light produced from the down-conversion process is emitted from the crystal in cones centered around the pump beam direction. The orientation of the pump beam

polarization with respect to the optical axis of the crystal determines the direction a particular wavelength will be emitted. The signal and idler photons are both emitted into their own cones, and if the cones are tangential to one another then the down-conversion is known as collinear—see Fig. 1.2(b). If the cones are spatially separated from one another then the down-conversion is called non-collinear—see Fig. 1.2(c). By increasing or decreasing the angle of the optical axis with respect to the pump beam polarization, one can increase or decrease the angle of separation of the two cones.

1.3   A TOUR THROUGH THIS WORK

Quantum entanglement plays a central role in the works of this dissertation. We can describe entanglement as a strong and inherently nonclassical correlation between two or more distinct physical systems. The quantum superposition principle says that "if an event can be realized in two or more distinguishable ways, the state of the system is a superposition of each way simultaneously". In this sense, the quantum entanglement is the superposition principle applied to certain nonlocal correlations: "If a correlation can be realized in two or more indistinguishable ways, the state of the system is a superposition of all such correlations simultaneously". It was first described in 1935 by one of the pioneers of quantum theory, Erwin Schrödinger, as "the distinguishing inherited characteristic of quantum mechanics" [25] and it was positioned at the heart of the famous EPR-paradox [26]. For many years, entangled states were considered the subject of philosophical arguments or were used only in experiments aimed at investigating the fundamental foundations of physics. For more than a decade, however, entangled states have become a central resource in the emerging field of quantum information science, which can be defined as the application of quantum physics phenomena to the storage, communication and processing of information. Quantum imaging offers numerous exciting opportunities in the area

8

of quantum information due to an intrinsic parallelism of optical image processing. In fact, it was shown in [27] that these two fields were two manifestations of the same principles. A quantum logic gate–the building block of a quantum computer and an optical Mach-Zehnder interferometer–the basic system of optical imaging, are formally equivalent and they represent the same phase measurement of a quantum system in two different realizations.

There are various approaches to quantum imaging and sensing in terms of the entangled sources of light. This dissertation focuses on the systems of quantum imaging and sensing using the sources of quantum-correlated photon-pairs produced by the process of parametric down-conversion. We present new theoretical results for enhancing the resolution and sensitivity of photon-photon correlation measurements in three different systems.

In the introduction chapter we give a brief overview of the systems of quantum imaging and sensing. First we introduce the standard limitations of the conventional imaging and sensing techniques using classical sources of light. Then we briefly outline the novelty of using quantum-correlated photons in interferometry, lithography, metrology and geometrical imaging.

In chapter 2, we show how the entangled photons produced by parametric down conversion can be used to improve the sensitivity of a Sagnac interferometer. The resolution of the Sagnac phase shift by the measurements of two-photon and four-photon coincidences increases by a factor of two and four respectively.

The entangled photon pairs have also very promising applications in quantum magnetometry. In chapter 3, we propose a method of measuring magnetic fields with increased resolution by using the magneto-optical rotations (MOR) of polarization entangled photon pairs. We demonstrate how the improvement in magneto-optical rotation of light could be realized by employing two different schemes with collinear and noncollinear down-conversion geometries. We calculate the resolution that can be

achieved in the MOR both by the use of coherent light and down-converted light. We discuss the possibility that the Heisenberg limit could be reached in magnetometry by the use of down-converted light.

In chapter 4, for a Mach-Zehnder type interferometer, we propose a new idea of using stimulated parametric processes along with spontaneous ones to produce resolution improvement while at the same time maintaining high visibility at large gains of the parametric process. We use coherent beams at the signal and the idler frequencies for the stimulation. We further show enhancement of the count rate by several orders when stimulated parametric processes are used. Both the two photon counts and the visibility can be controlled by the phases of the stimulating coherent beams.

Chapter 5 particularly focuses on the minimum phase sensitivity limit. We address the question of fundamental quantum limit in the phase sensitivity with the stimulated parametric down-conversion source which is proposed in chapter 4. We analyze the minimum phase uncertainty in a Mach-Zehnder type interferometer employing three different measurement schemes and compare the results with the standard quantum limit that is set for coherent sources.

In chapter 6 we summarize our results and give an outlook for the future possibilities to improve the ideas. Some appendices follow at the end where we present most of the longer calculations.

CHAPTER 2

SAGNAC INTERFEROMETRY WITH ENTANGLED PHOTONS

2.1 INTRODUCTION

When two electromagnetic waves counter-propagate along a circular path in rotation they experience different travel times to complete the path. This induces a phase shift between the two counter-propagating waves proportional to the angular velocity of the rotation. This phase difference is known as the Sagnac effect [28] and in addition to its scientific importance, it has numerous practical applications such as the detection and high-precision measurement of rotation. It was studied and used in optics only with lasers until the new work [29] where they demonstrated the single-photon interference in the fiber Sagnac interferometer using spontaneous parametric down conversion as the source of single photons. However, it turns out that the results of interference are no different than with classical sources. This is also true of many interferometric experiments done at the single photon level [30, 31, 32]. Thus a natural question would be—what is the nature of interference if we replace the single photon source by an entangled photon pair source. This is what we examine in detail. We find that the sensitivity of a Sagnac interferometer could be considerably improved by using correlated photons [19, 20]. We thus bring the Sagnac interferometer in the same class as other experiments on imaging [9, 21], lithography [1, 2, 22, 23, 33, 34] and spectroscopy [24].

Parametric down conversion (PDC) is the predominant mechanism for experimentalists to create entangled photon pairs as well as single photons. Multi-photon entangled states produced in the down-conversion process are often used in quan-

tum information experiments and applications like quantum cryptography and the Bell inequalities. In particular, demonstrations of two-photon [12, 13, 35, 36] and four-photon [37, 38] interferences are holding promise for realizable applications with entanglement-enhanced performance. The principle of this enhancement lies in the fact that "the photonic de Broglie wavelength" [39] of an ensemble of photons with wavelength λ and number of photons n can be measured to be λ/n using a special interferometer. Further Steuernagel [40] has proposed the measurement of the reduced de Broglie wavelength of two- and four-photon wave packets.

In this chapter, we present an analysis of how parametric down converted photons could be useful to increase the rotation sensitivity in Sagnac interferometers. The results show two- and four-fold increase in the sensitivity which can be interpreted as a sign of two- and four-photon interference effect. The organization of the chapter is as follows. The Sagnac ring interferometer is described in section 2.2 and the Sagnac phase shift is derived. In section 2.3, we analyze interference results with classical and quantum inputs. We compare the results obtained from entangled photon pairs input with classical and single-photon inputs. We show how the two-photon and four-photon coincidences increase the sensitivity in the phase shift. The visibility of the counts is also discussed. We conclude the chapter in section 2.4 with a brief discussion of the disturbances that can effect the transmission of modes in fibers.

2.2   THE SAGNAC INTERFEROMETER

The Sagnac interferometer consists of a ring cavity around which two laser light beams travel in opposite directions on a rotating base. One can form an interference pattern by extracting and heterodyning portions of the two counter-propagating beams to detect the rotation rate of the ring cavity relative to an inertial frame. The position of the interference fringes is dependent on the angular velocity of the setup. This dependence is caused by the rotation effectively shortening the path distance of one

beam, while lengthening the other. In 1926, a Sagnac interferometer has been used by Albert Michelson and Henry Gale to determine the angular velocity of the Earth. It can be used in navigation as a ring laser gyroscope, which is commonly found on fighter planes, navigation systems on commercial airliners, ships and spacecraft.
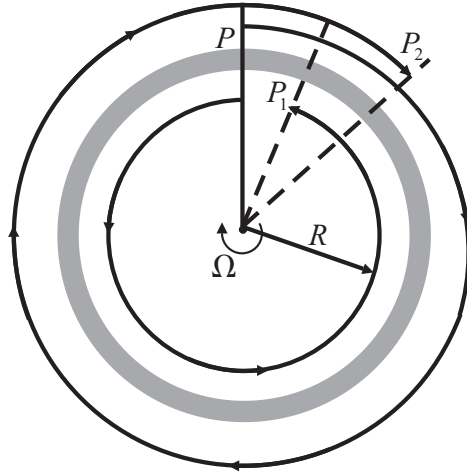
Figure 2.1: Schematics of a Sagnac ring interferometer.

The Sagnac effect [28] can be understood by considering a circular ring interferometer like the one shown in Fig. 2.1. The input laser field enters the interferometer at point P and is split into clockwise (CW) and counterclockwise (CCW) propagating beams by a beam splitter. If the interferometer is not rotating, the beams recombine at point P after a time given by

$$t = \frac{2\pi R}{c},$$
(2.1)

where R is the radius of the circular beam path. However, if the interferometer is rotating with angular velocity Ω, about an axis through the center and perpendicular to the plane of the interferometer, then the beams reencounter the beam splitter at different times. The transit times to complete one round trip for CW (t_2 at point P_2) and CCW (t_1 at point P_1) are given by,

$$t_1 = \frac{2\pi R}{c + R\Omega},$$
(2.2)

13

$$t_2 = \frac{2\pi R}{c - R\Omega} \ . \tag{2.3}$$

Then one round trip time delay between the two beams is the difference

$$\Delta t = t_2 - t_1 = \frac{4\pi R^2 \Omega}{c^2 - R^2 \Omega^2} \ . \tag{2.4}$$

For non-relativistic perimeter speeds (i.e. reasonable values of R and Ω), $R^2\Omega^2 \ll c^2$,

$$\Delta t = \frac{4\pi R^2 \Omega}{c^2} \ . \tag{2.5}$$

The angular phase difference between the two counter propagating waves, the Sagnac effect, can be written as,

$$\phi = \omega \Delta t = \frac{8\pi}{\lambda c} A\Omega \, , \tag{2.6}$$

where λ is the wavelength, c the light velocity in vacuum, A the interferometer area and Ω the angular velocity of the interferometer. A more general approach [42, 43, 44] shows that the phase shift does not depend on the shape of the interferometer and it is proportional to the flux of the rotation vector Ω through the interferometer enclosed area. Then one can increase the flux by using a multi-turn round-trip path like utilizing an optical fiber. In terms of the total length of the optical fiber, L, we can recast Eq. (2.6) into

$$\phi = \frac{4\pi L R \Omega}{\lambda c} \ . \tag{2.7}$$

Eq. (2.7) shows that the phase shift induced by rotation of a Sagnac fiber ring interferometer increases linearly with the total length of the optical fiber.

2.3 THE SAGNAC INTERFEROMETER WITH CLASSICAL AND QUANTUM INPUTS

2.3.1 Classical input

We now consider the Sagnac fiber ring interferometer setup shown in Fig. 2.2. The two input ports 1 and 2 are mixed by a 50/50 beam splitter and sent through a
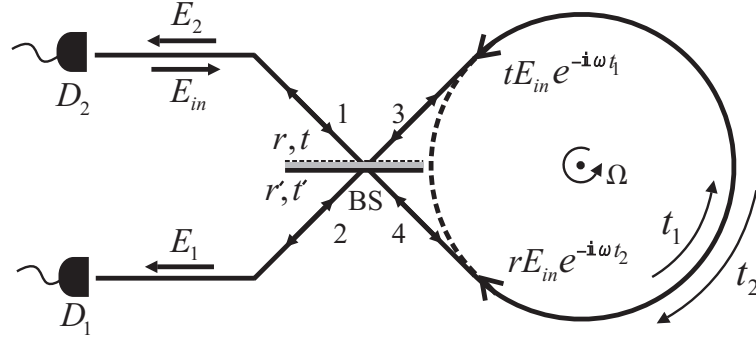
Figure 2.2: The Sagnac interferometer setup with classical input. The input field E_{in} is separated by the beam splitter into two counter-propagating waves tE_{in} and rE_{in}. Because of the rotation they end up at the beam splitter at different times (t_1, t_2).

rotating loop of fiber in the opposite direction. Then the beams recombine at the beam splitter and come out from the ports they entered. The rotation induces the phase difference ϕ given by the Eq. (2.7). If we choose the transmission and reflection coefficients of the beam splitter as $t = 1/\sqrt{2} = t'$, $r = i/\sqrt{2} = r'$ then the entire setup transforms the input field E_{in} into the output fields E_1 and E_2 by

$$\mathbf{E_1} = r'r\mathbf{E_{in}}e^{-i\omega t_2} + t^2\mathbf{E_{in}}e^{-i\omega t_1} = \mathbf{E_{in}}e^{-i\omega t_2}ie^{i\phi/2}\sin(\phi/2), \qquad (2.8)$$

$$\mathbf{E_2} = rt\mathbf{E_{in}}e^{-i\omega t_1} + t'r\mathbf{E_{in}}e^{-i\omega t_2} = \mathbf{E_{in}}e^{-i\omega t_2}ie^{i\phi/2}\cos(\phi/2), \qquad (2.9)$$

where ω is the frequency of the input field. The intensity measurements at the detectors D_1 and D_2 becomes

$$I_1 = |\mathbf{E_1}|^2 = |\mathbf{E_{in}}|^2\sin^2(\phi/2), \qquad (2.10)$$

$$I_2 = |\mathbf{E_2}|^2 = |\mathbf{E_{in}}|^2\cos^2(\phi/2), \qquad (2.11)$$

respectively.

Figure 2.3: The equivalent optical network diagram of the Sagnac interferometer for quantized fields. "ϕ" represents the phase shift provided by the rotating loop of the interferometer. The detectors D_3 and D_4 with the extra beam splitters (dashed lines) are to be used for four-photon coincidence counting.

2.3.2 Quantum inputs

Now we analyze the results with quantized fields. Fig. 2.3 shows the equivalent optical network diagram of the interferometer. We denote $\hat{a}_1$ and $\hat{a}_2$ as the input mode operators. The two beam splitters represent double-use of the actual beam splitter. The output modes $\hat{b}_1$ and $\hat{b}_2$ are related to the input modes by

$$
\begin{pmatrix} \hat{b}_1 \\ \hat{b}_2 \end{pmatrix} = \underbrace{\frac{1}{\sqrt{2}} \begin{pmatrix} 1 & i \\ i & 1 \end{pmatrix}}_{BS_{out}} \underbrace{\begin{pmatrix} 1 & 0 \\ 0 & e^{i\phi} \end{pmatrix}}_{SAGNAC} \underbrace{\frac{1}{\sqrt{2}} \begin{pmatrix} 1 & i \\ i & 1 \end{pmatrix}}_{BS_{in}} \begin{pmatrix} \hat{a}_1 \\ \hat{a}_2 \end{pmatrix},
$$

$$
= i e^{i\phi/2} \begin{pmatrix} -\sin(\phi/2) & \cos(\phi/2) \\ \cos(\phi/2) & \sin(\phi/2) \end{pmatrix} \begin{pmatrix} \hat{a}_1 \\ \hat{a}_2 \end{pmatrix}, \tag{2.12}
$$

where the global phase $ie^{i\phi/2}$ can be dropped. The use of a half-wave plate (HWP) is required when the input ports have polarizations orthogonal to each other. Now

16

the input and output modes are related to each other by the linear transformation,

$$\hat{b}_i = \sum_{j=1}^{2} S_{ij}\hat{a}_j, \tag{2.13}$$

where the matrix S of the coefficients S_{ij} is known as the scattering matrix associated with the network. In fact, Eq. (2.13) refers to the Heisenberg picture, where the state vectors are constant while operators evolve. Therefore, without knowing the Hamiltonian that describes the evolution by the unitary operator U on the state vectors, by using the dynamics of the operators

$$\hat{a}_i \rightarrow \hat{b}_i = \sum_{j=1}^{2} S_{ij}\hat{a}_j \equiv U^\dagger \hat{a}_i U, \tag{2.14}$$

$$\hat{a}_i^\dagger \rightarrow \hat{b}_i^\dagger = \sum_{j=1}^{2} S_{ij}^*\hat{a}_j^\dagger \equiv U^\dagger \hat{a}_i^\dagger U, \tag{2.15}$$

one can calculate the probabilities for detecting certain numbers of photons at certain outputs.

Now, let us analyze the rotation sensitivity to the phase shift "ϕ" for some Fock state inputs. We denote n-photons in mode $\hat{a}_1$ and m-photons in mode $\hat{a}_2$ by $|nm\rangle$. First, we begin with the input state $|10\rangle$, that is a single incident photon in mode $\hat{a}_1$ with the other mode in vacuum state. The output state can be written as

$$U|10\rangle = U\hat{a}_1^\dagger|00\rangle = U\hat{a}_1^\dagger U^\dagger U|00\rangle = U\hat{a}_1^\dagger U^\dagger|00\rangle. \tag{2.16}$$

The last equality results from the fact that the interferometer has no effect on the vacuum $|00\rangle$. Although we are in the Schrödinger picture, it is perfectly valid to use Eq. (2.15) with the substitution $U \rightarrow U^\dagger \equiv U^{-1}$. This implies $S \rightarrow S^\dagger$ resulting in

$$U\hat{a}_i^\dagger U^\dagger = \sum_{j=1}^{2} S_{ji}\hat{a}_j^\dagger. \tag{2.17}$$

If we substitute Eq. (2.17) into Eq. (2.16) and use the scattering matrix given by Eq. (2.12), we find

$$U|10\rangle = -\sin(\phi/2)|10\rangle + \cos(\phi/2)|01\rangle, \tag{2.18}$$

17

up to an overall phase. Similarly we can calculate

$$U|11\rangle = \frac{1}{\sqrt{2}}\sin(\phi)(-|20\rangle + |02\rangle) + \cos(\phi)|11\rangle, \tag{2.19}$$

where the input is a pair of photons, one at each of the ports 1 and 2.

2.3.3 Single-photon input vs. two-photon input

The Heisenberg picture is convenient for computing the expectation values of photon numbers. For the single photon input $|10\rangle$, the intensities at the detectors D_1 and D_2 read

$$I_1 \equiv \langle \hat{b}_1^\dagger \hat{b}_1 \rangle = \sin^2(\phi/2), \tag{2.20}$$

$$I_2 \equiv \langle \hat{b}_2^\dagger \hat{b}_2 \rangle = \cos^2(\phi/2), \tag{2.21}$$

whereas for the two-photon input $|11\rangle$, we have the single-photon counts at each detector $\langle \hat{b}_1^\dagger \hat{b}_1 \rangle = 1 = \langle \hat{b}_2^\dagger \hat{b}_2 \rangle$, i.e. there is no interference. On the other hand, by using Eq. (2.12), we can calculate the two-photon coincidences at the detectors D_1 and D_2,

$$I_{12} \equiv \langle \hat{b}_1^\dagger \hat{b}_2^\dagger \hat{b}_2 \hat{b}_1 \rangle = \cos^2(\phi), \tag{2.22}$$

which has a two-fold increase in the fringe pattern. This is also clear from the Schrödinger evolution of the state given by Eq. (2.19). The reason of this two-fold increase lies in the fact that when the two photons, one from each input port, enter into the loop, they transform into the following two-photon path-entangled state,

$$|11\rangle \rightarrow \frac{|20\rangle + |02\rangle}{\sqrt{2}} \rightarrow \frac{|20\rangle + e^{i2\phi}|02\rangle}{\sqrt{2}}, \tag{2.23}$$

which shows a two-fold reduction in the wavelength of source photons. This was nicely demonstrated in the experiment [36] using photon pairs (biphotons) generated by spontaneous PDC.

2.3.4 Entangled photon pairs

We now discuss how the results given by Eqs. (2.10) and (2.11) are modified under conditions of arbitrary pumping, if we work with down-converted photons. To avoid coupling losses to a fiber, entangled photon pairs can also be generated inside a fiber at telecom wavelengths. This has been demonstrated by Kumar and coworkers [41]. The state produced in nondegenerate parametric down conversion can be written as

$$|\psi\rangle = \frac{1}{\cosh g} \sum_{n=0}^{\infty} (-e^{i\theta} \tanh g)^n |n\rangle_1 |n\rangle_2. \qquad (2.24)$$

This state can be generated mathematically by applying the two-mode squeeze operator $\hat{S} = \exp(\rho^* \hat{a}_1 \hat{a}_2 - \rho \hat{a}_1^\dagger \hat{a}_2^\dagger)$ on the vacuum, where $\rho = g e^{i\theta}$ is the complex interaction parameter (also known as the squeezing parameter) proportional to the nonlinearity of the crystal, the pump amplitude and the crystal length. The polarizations of photon pairs in the noncollinear type-I and the collinear type-II down-conversion are the same and orthogonal respectively. At first glance, it is easy to see that this state is nonseparable ($\equiv$ entangled) to a product of states of mode 1 and mode 2. It is already in Schmidt-decomposed form with a Schmidt number higher than 1 for $g > 0$, which is a measure of entanglement [45]. Moreover one can calculate the *Entropy of Entanglement* [46], $E = -\mathrm{Tr}_2 \rho \log_2 \rho$ as a function of g,

$$E = \cosh^2 g \log_2(\cosh^2 g) - \sinh^2 g \log_2(\sinh^2 g). \qquad (2.25)$$

The amount of entanglement given by Eq. (2.25) is approximately linear in g showing that the state in Eq. (2.24) is fully entangled for $g \to \infty$.

When the input modes are in the state given by Eq. (2.24) the output detectors D_1 and D_2 read the single counts

$$I_1 \equiv \langle \hat{b}_1^\dagger \hat{b}_1 \rangle = \sinh^2 g = \langle \hat{b}_2^\dagger \hat{b}_2 \rangle \equiv I_2, \qquad (2.26)$$

which does not give any information on the rotation. On the other hand, the two-photon coincidence count, after subtracting independent counts, normalized over the

product of single counts at each detector becomes,

$$g_{12}^2 = \frac{\langle \hat{b}_1^\dagger \hat{b}_2^\dagger \hat{b}_2 \hat{b}_1 \rangle}{\langle \hat{b}_1^\dagger \hat{b}_1 \rangle \langle \hat{b}_2^\dagger \hat{b}_2 \rangle} - 1 = \cos^2(\phi) \coth^2 g, \qquad (2.27)$$

which is twice more sensitive to the rotation than the result in Eq. (2.20) with 100% visibility. The signal itself depends on g and it is most significant when $g \approx 1$. The regime with an interaction parameter value of $g = 1.39$ has already been reached in the experiment [47].

On the other hand, we can employ a different measurement—the projective measurement,

$$\begin{aligned} P_2 &= \text{Tr}[|11\rangle\langle 11|\rho(\phi)] \equiv |\langle 11|U|\psi\rangle|^2 \\ &= \frac{\tanh^2 g}{\cosh^2 g} \cos^2(\phi), \end{aligned} \qquad (2.28)$$

which is the probability of detecting two photons, one at each detector operating in coincidence. Here the state $\rho(\phi) = U|\psi\rangle\langle\psi|U^\dagger$ is the evolved density matrix corresponding to the state given in Eq. (2.24). This probability can be easily calculated by utilizing the Schrödinger picture evolution of the state vector $|11\rangle$ given in Eq. (2.19). The expression in Eq. (2.28) is a pure two-photon interference term since the phase runs twice faster than the source photons. Thus, the two-photon coincidences by using the state in Eq. (2.24) shows two-fold increase in the sensitivity of the phase measurement.

The next question is—can we increase the sensitivity further by measuring higher order coincidences? We suggest employing four single-photon detectors D_i ($i = 1, 2, 3, 4$) as depicted in Fig. 2.3. We note that in a recent experiment [48] the tomography of the Fock state $|2\rangle$ was done by letting the two photons propagate in different directions and by using single photon detectors. For detection of multi-photons, it is easier to use single photon detectors. We examine the coincidence of clicking of four detectors, i.e. the probability of the state $|1_{\hat{D}_1} 1_{\hat{D}_3} 1_{\hat{D}_2} 1_{\hat{D}_4}\rangle$ where $\hat{D}_i$'s denote the modes that go into the corresponding detectors. This requires the state in modes
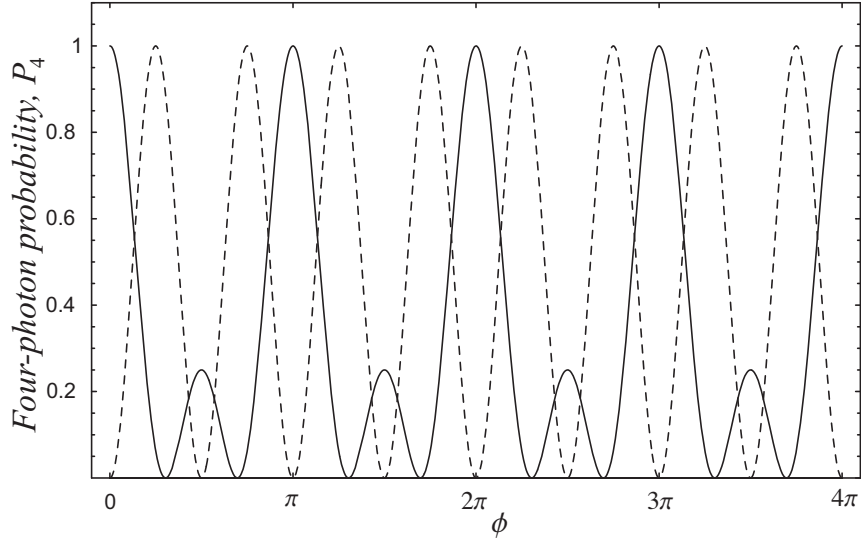
Figure 2.4: Normalized four-photon probability in coincidence in 2-by-2 (solid line) and 3-by-1 (dashed line) detection scheme described by Eqs. (2.32) and (2.34) respectively.

$\hat{b}_1$ and $\hat{b}_2$ before the beam splitters BS_1 and BS_2 to be in a four-photon subspace. We now outline this calculation. The four-photon coincidence detection probability is given by

$$
\begin{aligned}
P_4 &= |\langle 1_{\hat{D}_1} 1_{\hat{D}_3} 1_{\hat{D}_2} 1_{\hat{D}_4} | U_B U_S |\psi, 0_{\hat{v}_1} 0_{\hat{v}_2} \rangle|^2 \\
&= \langle 1_{\hat{D}_1} 1_{\hat{D}_3} 1_{\hat{D}_2} 1_{\hat{D}_4} | U_B U_S |\psi, 0_{\hat{v}_1} 0_{\hat{v}_2} \rangle \langle \psi, 0_{\hat{v}_1} 0_{\hat{v}_2} | U_S^\dagger U_B^\dagger | 1_{\hat{D}_1} 1_{\hat{D}_3} 1_{\hat{D}_2} 1_{\hat{D}_4} \rangle, \quad (2.29)
\end{aligned}
$$

where the state $|\psi, 0_{\hat{v}_1} 0_{\hat{v}_2} \rangle$ represents the tensor product of the state (2.24) with the vacuum ports v_1 and v_2 at the beam splitters BS_1 and BS_2. The unitary operators U_S and U_B represent the evolution of the states inside the Sagnac interferometer and the two beam splitters BS_1 and BS_2 respectively. First, we begin by calculating the inverse evolution

$$
\begin{aligned}
U_B^\dagger |1_{\hat{D}_1} 1_{\hat{D}_3} 1_{\hat{D}_2} 1_{\hat{D}_4} \rangle &= U_B^\dagger \hat{D}_1^\dagger \hat{D}_3^\dagger \hat{D}_2^\dagger \hat{D}_4^\dagger U_B U_B^\dagger |0000\rangle \\
&= (t_1^* \hat{b}_1^\dagger + r_1'^* \hat{v}_1^\dagger)(t_2^* \hat{b}_2^\dagger + r_2'^* \hat{v}_2^\dagger)(r_1^* \hat{b}_1^\dagger + t_1'^* \hat{v}_1^\dagger)(r_2^* \hat{b}_2^\dagger + t_2'^* \hat{v}_2^\dagger)|0000\rangle
\end{aligned}
$$

21

$$= t_1^* t_2^* r_1^* r_2^* \hat{b}_1^{\dagger 2} \hat{b}_2^{\dagger 2} |0000\rangle + \ldots, \tag{2.30}$$

where we take only four-photon state in modes $\hat{b}_1$ and $\hat{b}_2$ because other terms are irrelevant in our calculation. Here the t_i's and r_i's are the transmittance and reflectance coefficients of the beam splitters BS_i $(i = 1, 2)$. Next, we operate $U_S^\dagger$ on the resultant state above,

$$
\begin{aligned}
U_S^\dagger t_1^* t_2^* r_1^* r_2^* \hat{b}_1^{\dagger 2} \hat{b}_2^{\dagger 2} |0000\rangle &= t_1^* t_2^* r_1^* r_2^* U_S^\dagger \hat{b}_1^{\dagger 2} \hat{b}_2^{\dagger 2} U_S U_S^\dagger |0000\rangle \\
&= t_1^* t_2^* r_1^* r_2^* \left(-\sin(\phi/2)\hat{a}_1^\dagger + \cos(\phi/2)\hat{a}_2^\dagger \right)^2 \\
&\quad \times \left(\cos(\phi/2)\hat{a}_1^\dagger + \sin(\phi/2)\hat{a}_2^\dagger \right)^2 |0000\rangle \\
&= \left(\frac{1}{2}\sin(\phi)(-\hat{a}_1^{\dagger 2} + \hat{a}_2^{\dagger 2}) + \cos(\phi)\hat{a}_1^\dagger \hat{a}_2^\dagger \right)^2 |0000\rangle \\
&= \frac{1}{2}[1 + 3\cos(2\phi)]|2200\rangle + \ldots, \tag{2.31}
\end{aligned}
$$

where we use the transformation given by Eq. (2.12) between the modes $\hat{a}_1$, $\hat{a}_2$ and $\hat{b}_1$, $\hat{b}_2$. In the last line of Eq. (2.31) the first two modes are $\hat{a}_1$ and $\hat{a}_2$, while the last two modes are the vacuum modes of the beam splitters BS_1 and BS_2. In the last line of Eq. (2.31) we take only the state which has equal number of photons in modes $\hat{a}_1$ and $\hat{a}_2$ because the input state $|\psi\rangle$ is a pair photon state which is given in Eq. (2.24). Therefore the absolute square of the inner product of the resultant state given in the Eq. (2.31) with $|\psi, 0_{\hat{v}_1} 0_{\hat{v}_2}\rangle$ gives us the four-photon coincidence probability

$$P_4 = \frac{\tanh^4 g}{\cosh^2 g}|t_1 t_2 r_1 r_2|^2 \frac{1}{4}[1 + 3\cos(2\phi)]^2. \tag{2.32}$$

The result given by Eq. (2.32) shows a reduction in the period of fringes by developing smaller peaks as depicted in Fig. 2.4. The phase sensitivity shows a four-fold increase with respect to the result in Eq. (2.20) obtained by single-photon input.

The four-photon coincidence detection can be done in an alternative way as depicted in figure 2.5. Here, three of the four photons are to be detected in the upper output channel $\hat{b}_1$ while the fourth one goes into the detector placed in the lower output channel $\hat{b}_2$. This time, we place the two extra beam splitters BS_1 and BS_2 to
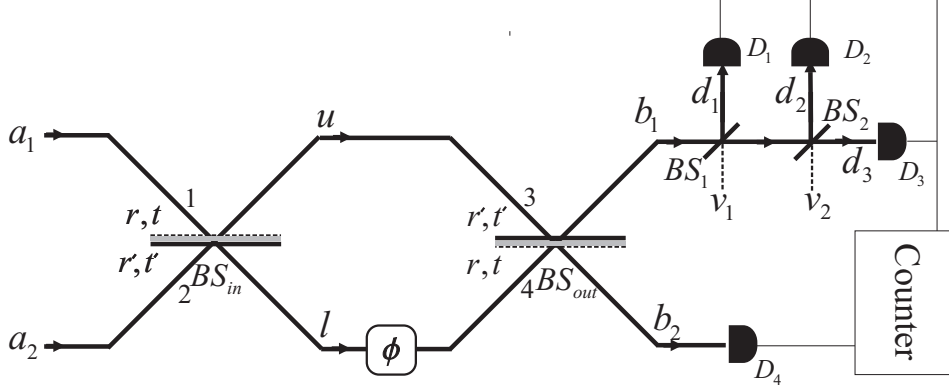
Figure 2.5: The Sagnac interferometer setup for four-photon coincidence detection in 3-by-1 scheme.

split up the three photons into single photons before they arrive at the detectors D_1, D_2 and D_3. Now, we begin with the evolution of the four-photon subspace term $|22\rangle$ provided by the input state $|\psi\rangle$,

$$
\begin{aligned}
|22\rangle &= \frac{\hat{a}_1^{\dagger 2}}{\sqrt{2}}\frac{\hat{a}_2^{\dagger 2}}{\sqrt{2}}|00\rangle \longrightarrow \frac{1}{2}\left(\frac{i\hat{u}^\dagger + \hat{l}^\dagger}{\sqrt{2}}\right)^2 \left(\frac{\hat{u}^\dagger + i\hat{l}^\dagger}{\sqrt{2}}\right)^2 |00\rangle \\
&\longrightarrow -\frac{1}{8}\left\{\left(\frac{i\hat{b}_1^\dagger + \hat{b}_2^\dagger}{\sqrt{2}}\right)^4 + e^{i4\phi}\left(\frac{\hat{b}_1^\dagger + i\hat{b}_2^\dagger}{\sqrt{2}}\right)^4 + 2e^{i2\phi}\left(\frac{i\hat{b}_1^\dagger + \hat{b}_2^\dagger}{\sqrt{2}}\right)^2\left(\frac{\hat{b}_1^\dagger + i\hat{b}_2^\dagger}{\sqrt{2}}\right)^2\right\}|00\rangle \\
&= \frac{1}{4}\left\{e^{i2\phi}\sin(2\phi)\hat{b}_1^{\dagger 3}\hat{b}_2^\dagger + \cdots\right\}|00\rangle \\
&\longrightarrow \frac{e^{i2\phi}}{4}\sin(2\phi)\left\{\left(r_1\hat{d}_1^\dagger + t_1(r_2\hat{d}_2^\dagger + t_2\hat{d}_3^\dagger)\right)^3 \hat{b}_2^\dagger\right\}|0000\rangle \\
&= \frac{e^{i2\phi}}{4}\sin(2\phi)\left\{6r_1 t_1^2 r_2 t_2 \hat{d}_1^\dagger \hat{d}_2^\dagger \hat{d}_3^\dagger \hat{b}_2^\dagger + \cdots\right\}|0000\rangle \\
&= \frac{3}{2}e^{i2\phi}\sin(2\phi)r_1 t_1^2 r_2 t_2 |1111\rangle.
\end{aligned}
\tag{2.33}
$$

The arrow in the first line represents the evolution of the input modes into the interferometer after BS_{in}, while the second arrow shows further evolution of the modes by the phase shift ϕ and BS_{out}. In the third line we omit the terms giving photons in the channels other than three in b_1 and one in b_2. The fourth line shows how the channel

$\hat{b}_1$ split up into the modes $\hat{d}_1$, $\hat{d}_2$ and $\hat{d}_3$ going into the detectors D_1, D_2 and D_3 respectively and since we are considering only one photon per detector we omit the other terms in the following line. In the last line we obtain the state corresponding to the four-photon coincidence detection in a 3-by-1 scheme. Then, we calculate the probability of four-photon coincidence to be,

$$P_4^{(3by1)} = \frac{\tanh^4 r}{\cosh^2 r}|t_1^2 t_2 r_1 r_2|^2 \frac{9}{4}\sin^2(2\phi). \tag{2.34}$$

The normalized plot of this probability is shown in Fig. 2.4. Note that all the peaks are even in the interference pattern showing a pure four-fold increase in the sensitivity. We note that Steuernagel has a similar result in his work [40] on reduced de Broglie wavelength using precisely two photon events at each detector. In our proposal above we use single photon detectors to do four-photon coincidence. Currently efforts are on to find efficient nonlinear absorbers so that these could be used for the detection of the precise number of photons [34, 49, 50].

2.4 CONCLUSION

There are advantages of using single photon interferometer as then the unwanted effects due to nonlinearities are avoided. However the integration time becomes long so that one can achieve the same level of sensitivity with classical interferometers [51]. What we are demonstrating is that we get super-resolution relative to what is obtained by the usage of single photons. We think that experiments should be feasible because many two-photon and four-photon interference effects have been observed [12, 13, 35, 36, 37, 38].

CHAPTER 3

TOWARDS THE HEISENBERG LIMIT IN MAGNETOMETRY WITH PARAMETRIC DOWN-CONVERTED PHOTONS

3.1 INTRODUCTION

In this chapter we present an analysis of how parametric down converted photons could be very useful in getting better spectroscopic information about the medium. We demonstrate how the improvement in magneto-optical rotation (MOR) of light could be realized by employing two different schemes with collinear and non-collinear type-II down conversion geometry compared to the use of coherent light. We calculate the resolution that can be achieved in the MOR's both by use of coherent light and down converted light. We discuss that the Heisenberg limit [52] could be reached in magnetometry by the use of down converted light.

3.2 MAGNETO-OPTICAL ROTATION (MOR) USING COHERENT LIGHT SOURCE

Consider single mode coherent light traveling in the z-direction and a linear isotropic medium made anisotropic by the application of magnetic field $\mathbf{B}$ in the z-direction. The incident field can be written in the form

$$\mathbf{E}(z,t) = \exp(-i\omega t + ikz)(\hat{\mathbf{x}}\varepsilon_x + \hat{\mathbf{y}}\varepsilon_y) + c.c. \tag{3.1}$$

The medium is described by the frequency and magnetic field dependent susceptibilities $\chi_\pm(\omega)$. That means the horizontally and vertically polarized components of the incident light will rotate on traveling in a medium of length l and the field at the exit

25

can be written as

$$\mathbf{E}(l,t) = \exp(-i\omega t + ikl)(\hat{\mathbf{x}}\varepsilon_{xl} + \hat{\mathbf{y}}\varepsilon_{yl}) + c.c. \tag{3.2}$$

The rotation of the horizontal and vertical components can be expressed by the relations

$$\begin{pmatrix} \varepsilon_{xl} \\ \varepsilon_{yl} \end{pmatrix} = R \begin{pmatrix} \varepsilon_x \\ \varepsilon_y \end{pmatrix} \tag{3.3}$$

where

$$R = e^{i\phi_+}e^{i\phi/2}\begin{pmatrix} \cos(\phi/2) & -\sin(\phi/2) \\ \sin(\phi/2) & \cos(\phi/2) \end{pmatrix}, \tag{3.4}$$

$$\phi = kl(\chi_+ - \chi_-), \tag{3.5}$$

$$\phi_+ = kl\chi_+. \tag{3.6}$$

The corresponding quantum mechanical description can be obtained by replacing the classical amplitudes ε_x and ε_y by the annihilation operators $\hat{a}_x$ and $\hat{a}_y$ respectively. For measurements with coherent sources one can look at the intensities of the x and y components of the output when the input is x polarized with coherent state amplitude α_x (See Fig. 3.1(a). Then the measured quantities will be

$$I_{xl} = \langle\hat{a}_{xl}^\dagger\hat{a}_{xl}\rangle = |\alpha_x|^2\cos^2(\phi/2), \tag{3.7}$$

$$I_{yl} = \langle\hat{a}_{yl}^\dagger\hat{a}_{yl}\rangle = |\alpha_x|^2\sin^2(\phi/2). \tag{3.8}$$

One can estimate the minimum detectable rotation angle ϕ_m by looking at the fluctuations ΔN_d in the photon number difference between horizontal and vertical photons, where the number difference operator is given as $N_d = \hat{a}_{yl}^\dagger\hat{a}_{yl} - \hat{a}_{xl}^\dagger\hat{a}_{xl}$. This expression is calculated to be $(\Delta N_d)^2 = |\alpha_x|^2\sin^2\phi$ and since the fluctuation noise is 1 we obtain $\phi_m \approx 1/\sqrt{\langle N\rangle}$ where $\langle N\rangle$ is the mean number of input photons which is equal to $|\alpha_x|^2$.
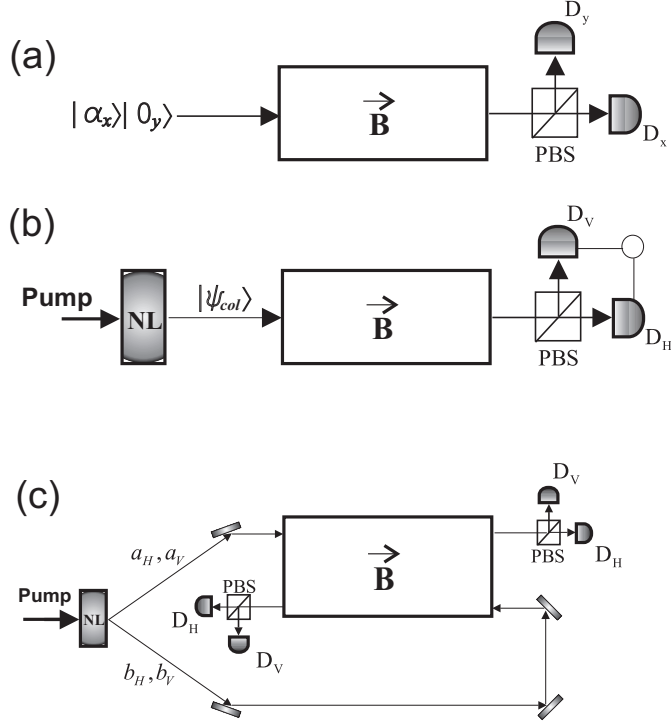
Figure 3.1: The setup for the Magneto-optical rotation of light by using (a) coherent source, type-II PDC photons with (b) collinear and (c) non-collinear geometry.

3.3 MOR USING COLLINEAR TYPE-II PDC AND TWO-PHOTON COINCIDENCE

We now discuss how the results (3.7) and (3.8) are modified if we work with down-converted photons. We first consider the collinear case shown in Fig. 3.1(b). The state produced in collinear PDC can be written as

$$|\psi_{col}\rangle = \frac{1}{\cosh g} \sum_{n=0}^{\infty} (-e^{i\psi} \tanh g)^n |n\rangle_H |n\rangle_V. \tag{3.9}$$

The values of the parameter g and the phase ψ are related to the pump amplitude of the nonlinear crystal that is used in the down conversion process and the coupling constant between the electromagnetic field and the crystal. Note that the state $|\psi_{col}\rangle$ is a superposition of n photon pairs of horizontally and vertically polarized modes. Inside the medium, these modes rotate with the same rotation matrix R given in Eq.

27

(3.4):

$$\begin{pmatrix} \hat{a}_{Hl} \\ \hat{a}_{Vl} \end{pmatrix} = R \begin{pmatrix} \hat{a}_H \\ \hat{a}_V \end{pmatrix}. \tag{3.10}$$

One can measure the intensity of each mode:

$$\begin{aligned} I_H &\equiv \langle \hat{a}_{Hl}^{\dagger} \hat{a}_{Hl} \rangle = \sinh^2 g \\ &= \langle \hat{a}_{Vl}^{\dagger} \hat{a}_{Vl} \rangle \equiv I_V. \end{aligned} \tag{3.11}$$

And the two-photon coincidence count is:

$$\begin{aligned} I_{HV} &\equiv \langle \hat{a}_{Hl}^{\dagger} \hat{a}_{Vl}^{\dagger} \hat{a}_{Hl} \hat{a}_{Vl} \rangle \\ &= \cos^2(\phi) \sinh^2 g \cosh^2 g + \sinh^4 g. \end{aligned} \tag{3.12}$$

Note the difference between Eqs. (3.7) and (3.12). With collinearly down-converted photons we measure a rotation angle that is twice as large compared with the angle for a coherent input. For $g \ll 1$ we obtain the same result as given in [24]. The fringe pattern and the visibility is given in Figs. 3.2 and 3.3. One can calculate the minimum detectable rotation angle again by looking at the fluctuations in the photon number difference N_d. This is given by $(\Delta N_d)^2 = 4 \sinh^2 g \cosh^2 \sin^2(\phi) = (1 + \langle N \rangle) \langle N \rangle \sin^2(\phi) \approx \langle N \rangle^2 \sin^2(\phi)$ for large $\langle N \rangle$ where $\langle N \rangle = 2 \sinh^2 g$. Making $(\Delta N_d) \sim 1$ [52] we get $\phi_m \approx 1/\langle N \rangle$. Note that the sensitivity of this quantity is also improved by a factor of $1/\sqrt{N}$.

3.4 MOR USING NON-COLLINEAR TYPE-II PDC AND FOUR-PHOTON COINCIDENCE

Next, we discuss the non-collinear PDC case. We have found an arrangement shown in Fig. 3.1(c) which is especially attractive for improving sensitivity. The entangled photons are coming in two different spatial modes, $\hat{a}$ and $\hat{b}$. While one mode (say $\hat{a}$) is going parallel to **B** inside the medium, the other is going anti-parallel to it. At the
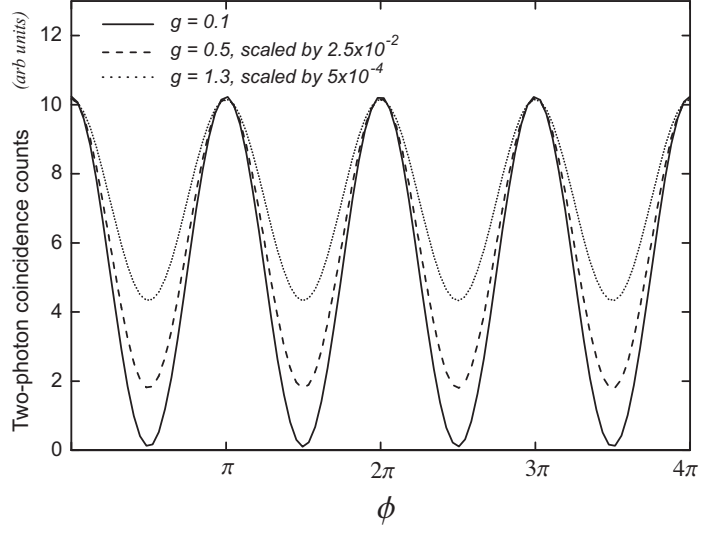
Figure 3.2: The MOR plot of two-photon coincidence counts defined by the Eq. (3.12) in collinear type-II PDC. g is the interaction parameter that defines the pumping strength used in the production of down converted photons and $\phi = kl(\chi_+ - \chi_-)$.
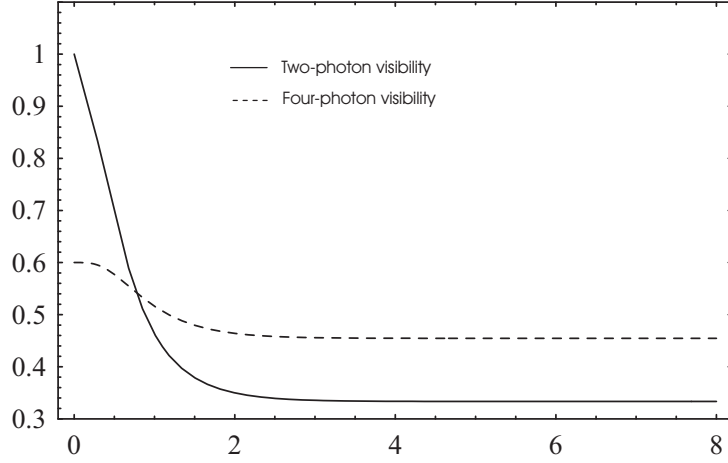
Figure 3.3: The visibility of two-photon and four-photon counts defined by the Eqs. (3.12) and (3.19) respectively.
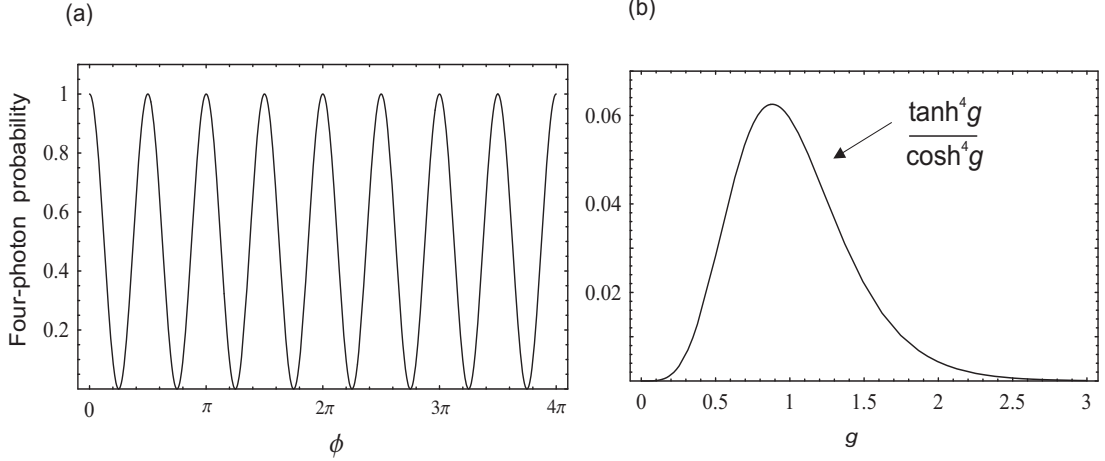
Figure 3.4: (a) The normalized four-photon probability defined in Eq. (3.17), and (b) its envelope with respect to the interaction parameter g in the non-collinear geometry.

exit we separate the H and V modes by polarizing beam splitters. The state of the input photons can be written in the form [53]

$$|\psi_{non}\rangle = \frac{1}{\cosh^2 g} \sum_{n=0}^{\infty} \sqrt{n+1}(\tanh g)^n |\psi_n\rangle, \qquad (3.13)$$

where

$$|\psi_n\rangle = \frac{1}{\sqrt{n+1}} \sum_{m=0}^{n} (-1)^m |n-m\rangle_{\hat{a}_H} |m\rangle_{\hat{a}_V} |m\rangle_{\hat{b}_H} |n-m\rangle_{\hat{b}_V}. \qquad (3.14)$$

Here $|m\rangle_{\hat{a}_V}$ represents m vertically polarized photons in mode $\hat{a}$. Inside the medium, " $+$ " and " $-$ " polarization components of the modes $\hat{a}$ and $\hat{b}$ gain phases $kl\chi_+$ and $kl\chi_-$ respectively. Thus we can write an effective Hamiltonian for the evolution of the state $|\psi_{non}\rangle$ inside the medium as follows:

$$H_{\mathrm{med}} = \chi_+ \hat{a}_+^\dagger \hat{a}_+ + \chi_- \hat{a}_-^\dagger \hat{a}_- - \chi_+ \hat{b}_+^\dagger \hat{b}_+ - \chi_- \hat{b}_-^\dagger \hat{b}_-, \qquad (3.15)$$

where

$$\hat{a}_\pm = \frac{1}{\sqrt{2}}(\hat{a}_H \pm i\hat{a}_V), \quad \hat{b}_\pm = \frac{1}{\sqrt{2}}(\hat{b}_H \pm i\hat{b}_V). \qquad (3.16)$$

The minus sign in front of the $\hat{b}_\pm$ modes comes from the fact that they are traveling

30
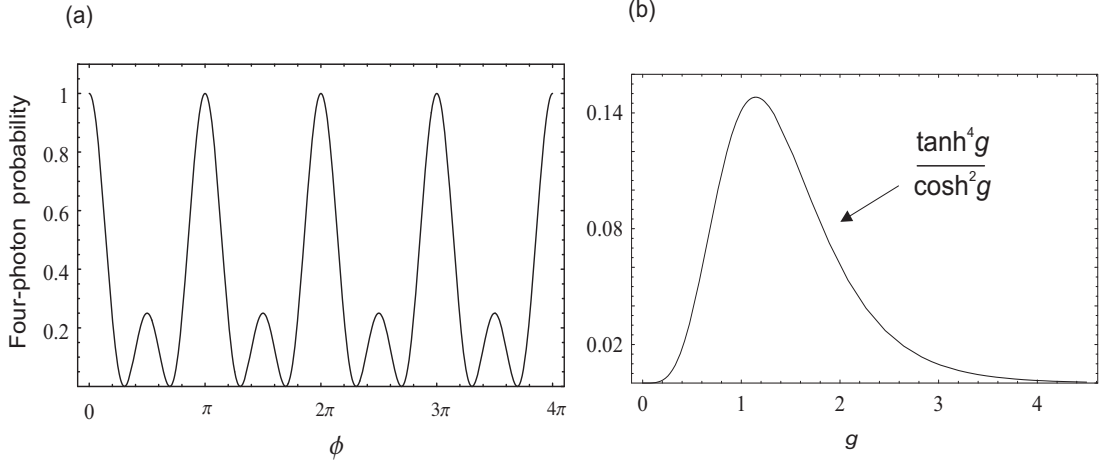
Figure 3.5: (a) The normalized four-photon probability defined in Eq. (3.18), and (b) its envelope with respect to the interaction parameter g at the exit ports of PBS in the collinear geometry.

anti-parallel to the **B** field inside the medium. Then one can calculate the probability of detecting four photons in each mode as:

$$
\begin{aligned}
P_{\text{non}} &= |\langle 1_{\hat{a}_H} 1_{\hat{a}_V} 1_{\hat{b}_H} 1_{\hat{b}_V}| \exp(-itH_{\text{med}})|\psi_{\text{non}}\rangle|^2 \\
&= \frac{\tanh^4 g}{\cosh^4 g} \cos^2(2\phi),
\end{aligned}
\tag{3.17}
$$

where t is the duration of the evolution of the state inside the medium. Note that this four-photon probability has a rotation angle that is four-times larger than the angle for a coherent input. The fringe pattern with respect to ϕ and the probability distribution with respect to g are shown in Fig. 3.4 (a) and (b).

Next we also examine the four-photon probability in the collinear case. The probability of finding two H-photons and two V-photons at the exit ports of the polarizing beam splitter is given by:

$$
\begin{aligned}
P_{\text{col}} &= |\langle 2_{\hat{a}_H} 2_{\hat{a}_V}| \exp(-itH_{\text{med}})|\psi_{col}\rangle|^2 \\
&= \frac{\tanh^4 g}{\cosh^2 g} \frac{1}{16}[1 + 3\cos(2\phi)]^2,
\end{aligned}
\tag{3.18}
$$

31
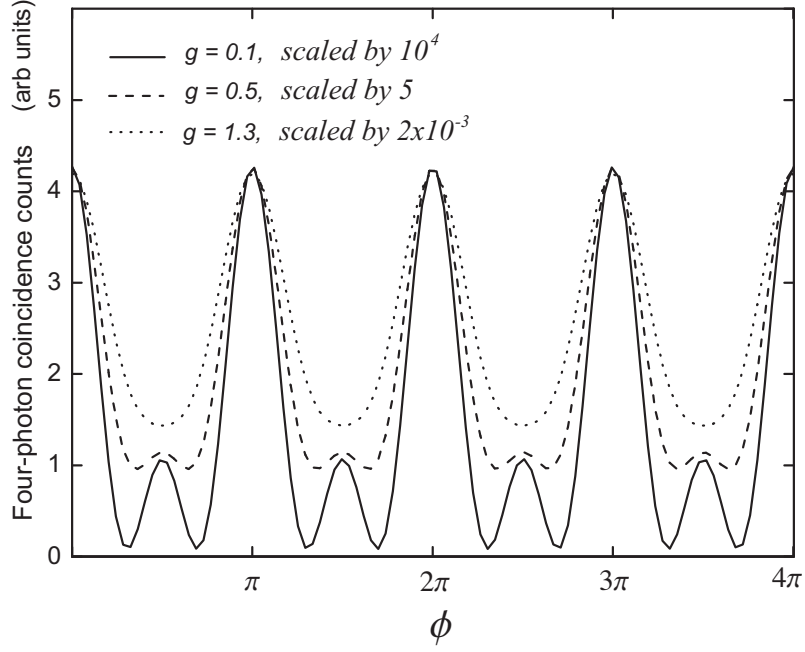
Figure 3.6: Four-photon coincidence counts defined in Eq. (3.19) with different interaction parameter values in the collinear geometry.

where we take $H_{\mathrm{med}} = \chi_+ \hat{a}_+^\dagger \hat{a}_+ + \chi_- \hat{a}_-^\dagger \hat{a}_-$ because of the collinear geometry. The normalized plot of this quantity with respect to the magneto-optical rotation angle ϕ and the envelope of the probability with respect to g are shown in Fig. 3.5 (a) and (b).

On the other hand one can also calculate the coincidence counts of four photons two-by-two at each detector as given by Glauber's higher order correlation functions:

$$
\begin{aligned}
I_{HHVV} &= \langle a_{Hl}^{\dagger 2} a_{Vl}^{\dagger 2} \hat{a}_{Hl}^2 \hat{a}_{Vl}^2 \rangle \\
&= (3\cos^2(\phi) - 1)^2 \sinh^4 g \cosh^4 g + 4(3\cos^2(\phi) + 1)\sinh^6 g \cosh^2 g \\
&+ 4\sinh^8 g. \tag{3.19}
\end{aligned}
$$

Plots of this quantity for different values of the interaction parameter g and the visibility are shown in Figs. 3.6 and 3.3. Note the distinction between Eqs. (3.18) and (3.19) which is a reflection of what the detector is set to measure as we explain now.

The former is the probability of the state $|\psi_{\text{col}}(t)\rangle$ to be projected onto the particular four-photon subspace $|22\rangle$, i.e. $\text{Tr}[|22\rangle\langle22|\rho_{\text{col}}(t)]$ where $\rho_{\text{col}}(t) = U|\psi_{\text{col}}\rangle\langle\psi_{\text{col}}|U^\dagger$ and U is the unitary operator that represents the evolution of the state by the Hamiltonian H_{med} in the collinear geometry. On the other hand, coincidence counting of four-photons at the detectors D_H and D_V (see Fig. 3.1(b)) is represented by the expectation value $\langle \hat{a}_H^{\dagger2}\hat{a}_V^{\dagger2}\hat{a}_H^2\hat{a}_V^2\rangle = \text{Tr}[\hat{a}_H^{\dagger2}\hat{a}_V^{\dagger2}\hat{a}_H^2\hat{a}_V^2\rho_{\text{col}}(t)]$. Note here that the operator $\hat{a}_H^{\dagger2}\hat{a}_V^{\dagger2}\hat{a}_H^2\hat{a}_V^2$ has the spectral decomposition $\sum_{nm}^\infty C_{nm}|nm\rangle\langle nm|$ and obviously it contains the projectors of all $(n+m)$-photon subspaces with nonzero coefficients C_{nm}. Therefore the four-photon counting process at detectors includes not only $|22\rangle$ but all other states $|nm\rangle$ in $|\psi_{\text{col}}(t)\rangle$. Here the state $|nm\rangle$ represents n and m photons in the $\hat{a}_H$ and $\hat{a}_V$ modes respectively.

3.5 CONCLUSION

We showed that the use of non-collinear type-II PDC light in MOR's increases the sensitivity by a factor of four in comparison with coherent light. We note that one can expect to have further flexibility in sensitivity by using suitably prepared atomic samples [54] as earlier studies [55, 56, 57] have shown how the sensitivity of interferometers can be improved by the use of entangled atoms.

We also give an argument that minimum rotation uncertainty scales to the Heisenberg limit by the use of down converted photons. It should be noted that the Heisenberg limit should be understood as an approximate limit at a large mean photon number, that is, the rotation uncertainty approaches the order of $1/\langle N\rangle$ for large $\langle N\rangle$ [20]. The regime with an interaction parameter value of $g = 1.3$ has already been reached in the experiment [58] giving entanglement of 12 photons and an evidence also was given for entanglement of up to 100 photons.

CHAPTER 4

QUANTUM IMAGING USING COHERENT BEAM STIMULATED PARAMETRIC DOWN-CONVERSION

4.1   INTRODUCTION

The question of beating the diffraction limit in optics has been the subject of extensive discussions recently [1, 19, 20, 22, 38, 40, 52, 59, 60, 61, 62, 63, 64, 65, 66, 67]. Dowling and coworkers proposed [1] a very new idea to improve the sensitivity of resolution by using detectors that work on two photon absorption and by using a special class of entangled states called $NOON$ states [59] . They showed that the diffraction limit can be beaten this way. The issue of the resolution in imaging continues to be addressed [2, 68, 69, 70, 71].

It is easy to produce $NOON$ states experimentally with two photons by using a very low gain parametric down converter. In this case the resolution is improved by a factor of two. However the probability of two photon absorption is very low unless one could develop extremely efficient two photon absorbers. One alternative would be to work with down converters in the high gain limit [72] however then the visibility of two photon counts goes down asymptotically to 20% [22]. Clearly we need to find methods that can overcome the handicap of having to work with smaller visibility. Another difficulty is with the magnitude of two photon counts. One needs to improve the intensity of two photon counts considerably.

In this chapter, we propose a new idea using stimulated parametric processes along with spontaneous ones to produce resolution improvement while at the same time maintaining high visibility at large gains of the parametric process. The stimulated

processes enhance the count rate by several orders of magnitude. We use coherent beams at the signal and the idler frequencies. We further find that the phases of coherent fields can also be used as tuning knobs to control the visibility of the pattern. It may be borne in mind that the process of spontaneous parametric down conversion has been a work horse for the last two decades in understanding a variety of issues in quantum physics and in applications in the field of imaging [10, 11, 12, 13, 14].

We expect that the use of stimulated processes along with spontaneous ones would change our landscape as far as fields of imaging and quantum sensors are concerned.

4.2 TWO-PHOTON COINCIDENCE COUNTS WITH STIMULATED PARAMETRIC DOWN-CONVERSION

We now describe the idea and the results of calculations that support the above assertion. Consider the scheme shown in Fig. 4.1. Here $\hat{a}_1$ and $\hat{b}_1$ are the signal and
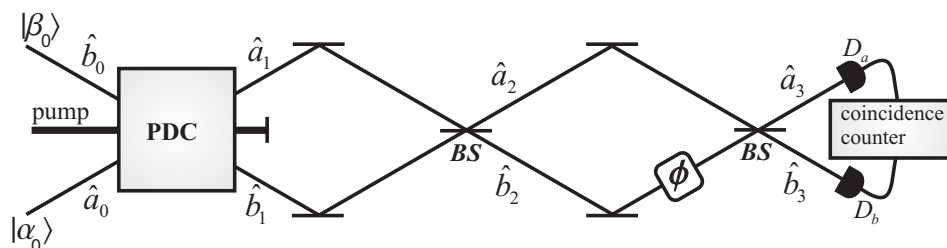
Figure 4.1: Using an input from non-degenerate stimulated parametric down-conversion for determination of phase via photon-photon correlations.

idler modes driven by the coherent fields. The usual case of spontaneous parametric down conversion is recovered by setting $\alpha_0 = \beta_0 = 0$. The ϕ is the phase introduced by the object or by an interferometer. For down conversion of type II the signal and idler would be two photons in two different states of polarization. In order to calculate the coincidence count it is good to work with Heisenberg operators. The

35

fields reaching the detectors are related to the input vacuum modes $\hat{a}_0$ and $\hat{b}_0$ via

$$\begin{pmatrix} \hat{a}_3 \\ \hat{b}_3 \end{pmatrix} = \frac{1}{\sqrt{2}} \begin{pmatrix} 1 & i \\ i & 1 \end{pmatrix} \begin{pmatrix} 1 & 0 \\ 0 & e^{i\phi} \end{pmatrix} \frac{1}{\sqrt{2}} \begin{pmatrix} 1 & i \\ i & 1 \end{pmatrix} \begin{pmatrix} \mu(\hat{a}_0 + \alpha_0) + \nu(\hat{b}_0^\dagger + \beta_0^*) \\ \mu(\hat{b}_0 + \beta_0) + \nu(\hat{a}_0^\dagger + \alpha_0^*) \end{pmatrix}, \quad (4.1)$$

where μ and ν are given in terms of the gain parameter g,

$$\mu = \cosh g, \quad (4.2)$$

$$\nu = e^{i\psi} \sinh g. \quad (4.3)$$

and ψ is the phase of the pump. We first note that in the absence of the object or $\phi = 0$, the mean count, say, at the detector D_a is given by

$$I_{\hat{a}} \equiv \langle \hat{a}_3^\dagger \hat{a}_3 \rangle = \sinh^2 g + |\alpha_0|^2 \left[1 + 2 \sinh^2 g + \sinh 2g \cos(\psi - 2\theta) \right], \quad (4.4)$$

where for simplicity we assume that $\alpha_0 = \beta_0$. We denote θ as the phase of α_0. Note that the first term in Eq. (4.4) is the intensity of spontaneously produced photons. The g-independent term in the square bracket is just the intensity of the coherent beam and the rest of the terms result from stimulated parametric down conversion. Note further that the mean count depends on the phase of the coherent beams used to produce stimulated down conversion.

Now, using our basic equation (4.1) we calculate the two-photon coincidence counts as follows:

$$I_{\hat{a}\hat{b}} \equiv \langle \hat{a}_3^\dagger \hat{b}_3^\dagger \hat{b}_3 \hat{a}_3 \rangle = A \left\{ 1 + \frac{V}{1 - V} \left(1 + \cos(2\phi) \right) \right\}. \quad (4.5)$$

Here V is the visibility of two-photon coincidence counts

$$V = \frac{B}{A + B}, \quad (4.6)$$

where

$$A = \sinh^4 g + 2|\alpha_0|^2 \sinh^2 g \left[1 + 2 \sinh^2 g + \sinh 2g \cos(\psi - 2\theta) \right], \quad (4.7)$$

$$\begin{aligned} B = \frac{1}{2} \Big\{ & \left(1 + \sinh^2 g \right) \sinh^2 g + |\alpha_0|^2 \sinh 2g \left[\sinh 2g + \left(1 + 2 \sinh^2 g \right) \cos(\psi - 2\theta) \right] \\ & + |\alpha_0|^4 \left[1 + 2 \sinh^2 g + \sinh 2g \cos(\psi - 2\theta) \right]^2 \Big\}. \end{aligned} \quad (4.8)$$

36

Both A and B depend on the gain g, amplitude and phase of the stimulating beams. In Figs. $4.2(a)$ and $4.2(b)$ we display the fringes in two-photon counts under different
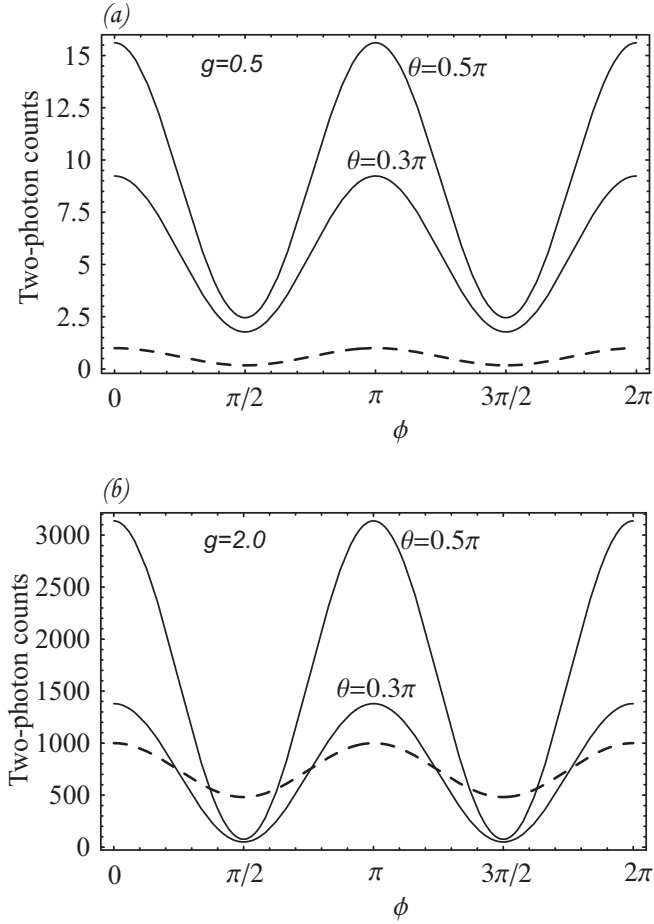
Figure 4.2: (a) Stimulated emission enhanced two-photon counts for various phases of the coherent field at the gain $g = 0.5$. The horizontal line shows the interferometric phase. The pump phase ψ is fixed at π. The counts are in units of two-photon coincidence rates coming from spontaneous down-conversion process. The modulus of the coherent field $|\alpha|$ is chosen such that the coincidences coming from SPDC and the coherent fields are equal to each other. The dashed line shows the two-photon counts for the case of a spontaneous process. (b) The same as (a), but at the gain $g = 2.0$. Here, the counts for the case of a spontaneous process (dashed line) is multiplied by a factor of 10^3.

conditions on the gain of the down-converter and the strength and phase of the stimulating beams. These figures clearly show the advantages of using stimulating parametric processes in quantum imaging. We next quantify these advantages.

We first note that in the absence of stimulating fields ($|\alpha_0| \to 0$)

$$V \longrightarrow \frac{1 + \sinh^2 g}{1 + 3\sinh^2 g},$$
(4.9)

and the strength of the two-photon counts reduces to

$$I_{\hat{a}\hat{b}} \longrightarrow 2\sinh^4 g + \sinh^2 g.$$
(4.10)

In the limit of large gain, the visibility drops to $1/3$ and the strength of two-photon counts goes as $\exp(4g)$. Next, we examine the effect of stimulated parametric processes on the visibility and the numerical strength of two-photon coincidence count. In the limit of large gain, the visibility of the stimulated process reads

$$V \longrightarrow \frac{\frac{1}{4} + |\alpha_0|^2\left(1 + \cos(\Delta)\right) + |\alpha_0|^4\left(1 + \cos(\Delta)\right)^2}{\frac{3}{4} + 3|\alpha_0|^2\left(1 + \cos(\Delta)\right) + |\alpha_0|^4\left(1 + \cos(\Delta)\right)^2},$$
(4.11)

where Δ is the phase difference, $\psi - 2\theta$, between the pump and stimulating (coherent) beams. Note that when $|\alpha_0| \to 0$ we recover the same result as Eq. (4.9). The visibility given in Eq. (4.11) has terms that arise from the interference between the spontaneous and the stimulated down-converted photons. Clearly we can control the value of the visibility by changing the amplitude of the stimulating beams. For example, we can obtain 60% visibility even for $|\alpha_0|^2 \sim 1$ if $\Delta = 0$, which should be compared with the 33% value in the absence of the stimulating beams. As we increase the stimulating beam intensity to ~ 10, we obtain 90% visibility. If we assume that the stimulating field's intensity is of the order of the number of spontaneous photons produced by the down-converter, i.e. $|\alpha_0|^2 \sim \sinh^2 g$, then the visibility of 100% can be reached at $g \simeq 2 - 2.5$ (For $\Delta = \pi$ we lose the advantage of a stimulating beam to produce

higher visibility.). In Fig. 4.3 we show the visibility of two-photon coincidences with respect to the gain for different values of the stimulating beam phases. The results in
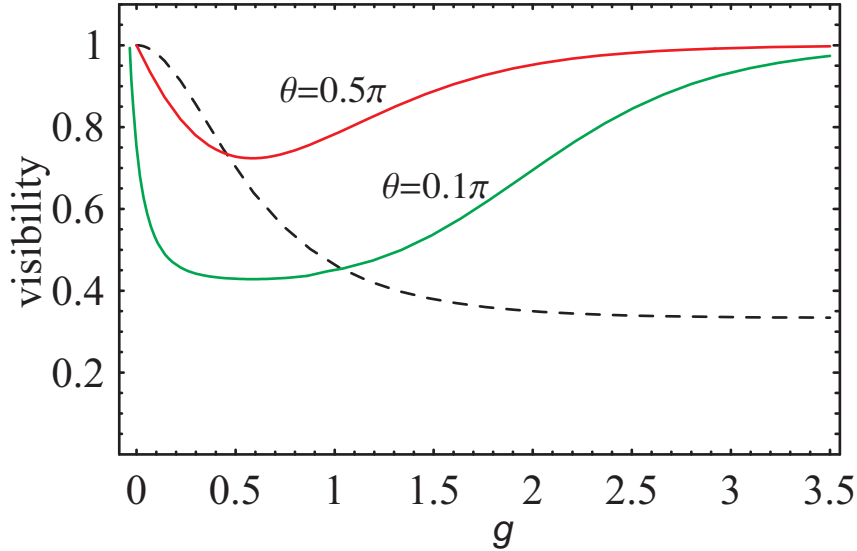
Figure 4.3: (Color online) Stimulated emission enhanced visibility of two-photon counts for various phases (red and green lines) of the coherent field with respect to the gain g. The pump phase ψ is fixed at π. The modulus of the coherent field $|\alpha_0|$ is chosen such that the coincidences coming from SPDC and the coherent fields are equal to each other. The dashed line shows the visibility of two-photon counts in the case of photons produced by spontaneous parametric down-conversion.

the region of large gain follow the approximate results based on Eq. (4.11).

We next examine the strength of two-photon counts in the limit of high gain. This depends on the interferometric phase ϕ. To get an estimate of the strength of two-photon counts let us set $\phi = 0$:

$$I_{\hat{a}\hat{b}} \longrightarrow 2\sinh^4 g\left\{1 + 4|\alpha_0|^2\left(1+\cos(\Delta)\right)+2|\alpha_0|^4\left(1+\cos(\Delta)\right)^2\right\}. \qquad (4.12)$$

Note that when $\alpha_0 = 0$ we recover Eq. (4.10). For $\Delta = 0$, the highest order term in Eq. (4.12) goes as $\exp(4g)|\alpha_0|^4$, i.e. a factor of $|\alpha_0|^4$ appears here compared to

the spontaneous process. This then reduces to $I_{\hat{a}\hat{b}} \to \exp(8g)$ if we assume that the stimulating field's intensity is of the order of the number of spontaneous photons produced by the down-converter, i.e. $|\alpha_0|^2 \sim \sinh^2(g)$. This leads to an enhancement by $\exp(4g)$ in the two-photon count rates compared to the case of spontaneous processes. In Figs. 4.4(a) and 4.4(b), we show the ratio of two-photon counts coming from the stimulated process to the spontaneous process both at the low and high gain limits respectively. It is shown that at $g \simeq 1.7$, three orders of magnitude rate enhancement
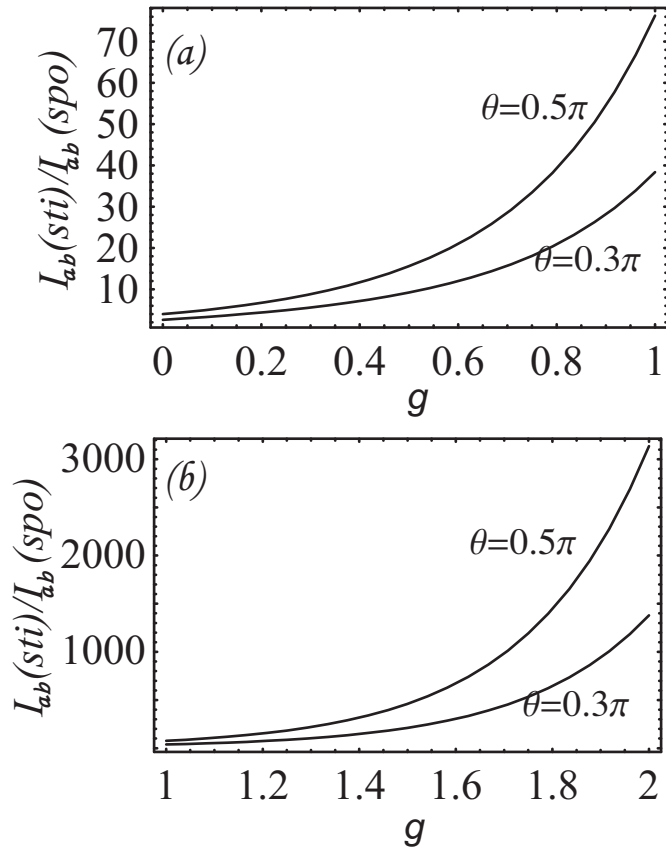
Figure 4.4: The ratio of the two-photon coincidences coming from the stimulated process to the spontaneous process for various phases of the coherent beams at the (a) low and (b) high gain limits respectively. The pump phase is fixed at π and the modulus of the coherent field $|\alpha|$ is chosen such that the coincidences coming from SPDC and the coherent fields are equal to each other.

is being reached. Therefore, in the determination of interferometric phase, we obtain a ground-breaking enhancement in both the visibility and the strength of the two-photon coincidence counts by controlling the phase and the amplitude of the stimulating coherent beams. We show in Figs. 4.2(a) and 4.2(b), this cumulative enhancement in both the visibility and the strength in the low and high gain limits respectively.

A question that we have not investigated in the present chapter concerns the minimum value of the phase $\Delta\phi$ that can be measured. In the literature one has the well known shot noise limit ($\Delta\phi \sim 1/\sqrt{N}$; where N is the total number of photons) obtained with coherent sources. This is to be compared with the Heisenberg limit ($\Delta\phi \sim 1/N$) obtained with sources prepared in special states and with very special detection schemes. Thus to improve the sensitivity it would be especially interesting if one can do the latter with photon numbers of the same order as in coherent sources. However so far one has achieved the Heisenberg limit only with photon numbers of order few. Thus the real question is—what is the achievable phase uncertainty given the presently available sources and measurement techniques? This is something that needs to be studied in depth. In the next chapter, we analyze the minimum phase uncertainty achievable with stimulated down-converted photons.

4.3   CONCLUSION

In conclusion, we have shown that using stimulated parametric processes along with spontaneous ones leads to resolution improvement and high signal values while at the same time maintaining high visibility at large gains of the parametric process. We use coherent beams at the signal and idler frequencies. We find that the phases of coherent fields can also be used as tuning knobs to control the visibility of the pattern. The use of stimulated parametric down-conversion also improves the rates of two-photon absorption in quantum lithography. The use of stimulated processes

in multi-photon coincidence events is expected to produce even bigger advantages, for example in producing much higher count rates. We hope to examine these in the future. Finally we believe that the use of stimulated processes along with spontaneous ones would change our landscape as far as the fields of imaging and quantum sensors are concerned.

CHAPTER 5

PHASE SENSITIVITY OF QUANTUM INTERFEROMETRIC SENSORS WITH REALISTIC ENTANGLED SOURCES

5.1   INTRODUCTION

The phase measurement through interference presents itself in many areas of physics as well as being a research subject by itself in quantum optics. The precise measurement of the optical phase at the quantum level is an issue of fundamental importance for both theory and experiment. The development of new physical theories depends on increasingly precise measurements. For example, extremely accurate methods of measuring the optical phase through interferometry are required for gravitational wave detection experiments [67, 73, 74, 75].

An optical interferometer typically has two input ports and two output ports. The quantity to be measured, usually a phase shift, is determined by measuring the difference in the number of photons emerging from the two output ports. The minimum phase shift, $\Delta\phi$, which one can measure, or the accuracy of the interferometer, is determined by the fluctuations in the input light. If a coherent state is sent into one of the ports and the vacuum into the other, then the accuracy is $1/\sqrt{N}$, where N is the mean number of photons in the input state. This is usually called the shot noise limit or the standard quantum limit (SQL). If a vacuum squeezed state with squeezing parameter $g > 0$ is sent into the second port instead of the vacuum, then the accuracy becomes $e^{-g}/\sqrt{N}$ [17]. Caves [17], as well as Bondurant and Shapiro [76] demonstrated that by feeding suitably constructed squeezed states into both ports of the interferometer the phase sensitivity can asymptotically approach $1/N$, for large

43

N. The increased accuracy by squeezing the vacuum port has been experimentally demonstrated [77, 78]. This phase sensitivity, which is inversely proportional to the total number of photons involved, is known as the Heisenberg limit and it is proven to be the fundamental (unsurpassable) quantum limit for the phase measurement [5]. Using squeezed light at the input ports is not the only method to beat the SQL of the phase measurement. It is also possible to reach the Heisenberg limit by using entangled photons as the two modes of the interferometer. For example, by using path entangled photons in a special $NOON$ state superposition [60]

$$|\Psi\rangle = \frac{1}{\sqrt{2}}(|N0\rangle + |0N\rangle),\tag{5.1}$$

together with special detection schemes ($\hat{M} = |N0\rangle\langle 0N| + |0N\rangle\langle N0|$), one can reach the Heisenberg limited accuracy in phase. Moreover, this state decreases the geometric distance between the two points that can be distinguished N times that of Rayleigh resolution limit.

It is easy to produce $NOON$ states experimentally with two photons by using a very low gain parametric down converter. However, preparation and detection mechanisms get extremely difficult for higher N. It requires very high order nonlinear materials with unrealistic measurement schemes. The Heisenberg limit accuracy using $NOON$ states can have a breakthrough in the phase measurement provided N is of the order of photon intensity produced in conventional laser sources. In the near future technology, to produce entangled photons of high intensity at the level of today's optical interferometers seems very unlikely. Therefore, it is desirable to analyze the sensitivity of phase using sources of stimulated processes that can reach high intensity of nonclassical photons. In the previous chapter, we have shown how the use of stimulated parametric down conversion processes could be advantageous for increasing resolution with high visibility and count rate. In this chapter we ask the question of phase accuracy of the proposed method by using various detection mechanisms. We calculate the phase sensitivity by using stimulated parametric down converted

44

photons for different realistic measurement schemes.

The organization of the chapter is as follows. In section I, we introduce the interferometer with the input photons coming from the stimulated parametric down-conversion process. The input-output relations between the modes of the interferometer are given. In Section II, we briefly introduce the fundamental sensitivity limit of the optical interferometers with quantum correlated photons. In section III, we calculate the minimum phase errors for three different measurement schemes.

5.2   THE INTERFEROMETER

We consider the Mach-Zehnder interferometer depicted in Fig. 5.1, which is the most widely used two-beam interferometer for optical phase measurements. The two beam splitters (BS) are used to mix the two input beams before and after the extra phase shift, ϕ, introduced into one of the optical paths. In our particular setup $\hat{a}_1$ and $\hat{b}_1$ are the input beams to the interferometer generated by the down-converting crystal. These signal and idler modes ($\hat{a}_1$ and $\hat{b}_1$ respectively) are driven by the coherent fields α_0 and β_0 which are represented by the modes $\hat{a}_0$ and $\hat{b}_0$ respectively. The usual case of spontaneous parametric down conversion is recovered by setting $\alpha_0 = \beta_0 = 0$. The output beams, $\hat{a}_3$ and $\hat{b}_3$, after the second beam splitter are then used for various types of photon intensity or correlation measurements. The relative phase change between the two paths inside the interferometer can be introduced by a different refractive index material or by changing the path lengths. This relative phase change can be detected through photon intensity measurement at the exit ports.

We now give the transformations between the input and the output modes of the interferometer. The fields reaching the detectors are related to the input modes $\hat{a}_1$ and $\hat{b}_1$ via

$$\begin{pmatrix} \hat{a}_3 \\ \hat{b}_3 \end{pmatrix} = \frac{1}{\sqrt{2}} \begin{pmatrix} 1 & i \\ i & 1 \end{pmatrix} \begin{pmatrix} 1 & 0 \\ 0 & e^{i\phi} \end{pmatrix} \frac{1}{\sqrt{2}} \begin{pmatrix} 1 & i \\ i & 1 \end{pmatrix} \begin{pmatrix} \hat{a}_1 \\ \hat{b}_1 \end{pmatrix}. \tag{5.2}$$
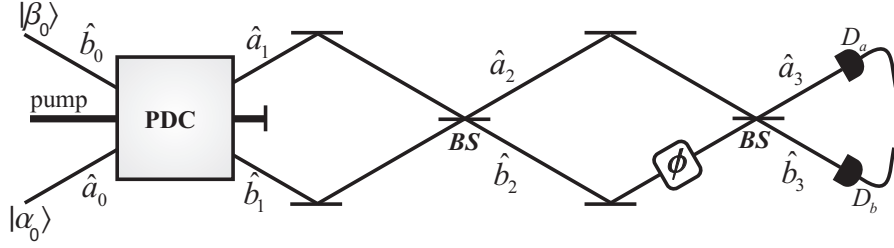
Figure 5.1: Mach-Zehnder interferometer using an input from stimulated parametric down-conversion for determination of phase.

In our particular setup, since the input modes are generated by the stimulated parametric down-conversion driven by the coherent fields, we further relate $\hat{a}_1$ and $\hat{b}_1$ to the vacuum modes of the down-conversion process, namely $\hat{a}_0$ and $\hat{b}_0$, by means of

$$\hat{a}_1 = \mu(\hat{a}_0 + \alpha_0) + \nu(\hat{b}_0^\dagger + \beta_0^*), \tag{5.3}$$

$$\hat{b}_1 = \mu(\hat{b}_0 + \beta_0) + \nu(\hat{a}_0^\dagger + \alpha_0^*), \tag{5.4}$$

where μ and ν are given in terms of the gain parameter g,

$$\mu = \cosh g, \tag{5.5}$$

$$\nu = e^{i\psi} \sinh g. \tag{5.6}$$

and ψ is the phase of the pump. It is easy to work with the Heisenberg operators in order to calculate the photon counts. The transformations given by Eq. (5.2) together with (5.3) and (5.4) give the evolution of the input modes in the Heisenberg picture.

5.3 SENSITIVITY

The traditional argument for the sensitivity limit of the phase measurement comes from the Heisenberg uncertainty relation for the phase and photon number [79, 80],

$$\Delta\phi\Delta N \geq 1, \tag{5.7}$$

where $\Delta\phi$ and ΔN are the fluctuations for the phase and photon number, respectively. The quantum mechanical definition of the fluctuation of an observable A is given by

$$\Delta A = \sqrt{\langle A^2 \rangle - \langle A \rangle^2}. \tag{5.8}$$

For example, the number fluctuation, ΔN, for the coherent state is $\sqrt{N}$ where N is the mean number of photons per unit time. Therefore, for shot-noise limited light, the optimum phase resolution is

$$\Delta\phi = \frac{1}{\sqrt{N}}. \tag{5.9}$$

It is clear from this expression that with an unlimited amount of energy, we can obtain phase measurements with an arbitrary accuracy, since by increasing the power the phase resolution becomes smaller. However, at very high powers, radiation pressure on the interferometer mirrors and heating induced effects add additional noise which eventually will limit the overall performance of the interferometer. On the other hand, quantum mechanics does not set any restriction on the fluctuation ΔN of the photon number. Intuitively, one would argue that because of energy constraint, ΔN should be bounded by the mean number of photons, that is $\Delta N \sim O(N)$. In fact, it has been proven that the ultimate precision in phase measurements is the so-called Heisenberg limit [5]

$$\Delta\phi \geq \frac{1}{N}, \tag{5.10}$$

where N is the total number of photons involved in the measurement. For optical laser interferometers operating at milliwatts of optical power, this quantum sensitivity boost corresponds to an eight-order-of-magnitude improvement of signal to noise. However, this requires a very high number of entangled photons of the order $\sim 10^{18}$. Current technology can utilize only 4 entangled photons at a time [38].

5.4 PHASE SENSITIVITY CALCULATIONS FOR STIMULATED PARAMETRIC DOWN-CONVERTED PHOTONS

To obtain the minimum limit of the phase sensitivity by the Heisenberg uncertainty relation in a particular measurement, we need to calculate fluctations of the phase and the number operator. However, there is no well defined Hermitian phase operator for some mathematical reasons. Instead, we measure a phase dependent Hermitian operator $\hat{X}$ such that

$$\Delta\phi = \frac{\Delta\hat{M}}{|\partial\langle\hat{M}\rangle/\partial\phi|}, \tag{5.11}$$

where $\Delta\hat{M}$ is the fluctuation of the operator $\hat{X}$ defined by Eq. (5.8).

A simple argument for the validity of this equation (5.11) can be given as follows [19]. Consider a differentiable function $y = y(x)$. We have $y'(x) = dy/dx \cong \Delta y/\Delta x$. The approximation becomes an equality in the limit $\Delta x \to 0$. However, if $y(x)$ is a fluctuating dependent random variable, then we cannot take $\Delta y \to 0$. Hence the best we can resolve the independent variable x is to within the associated Δx. Hence, given Δy, the minimal resolvable Δx is given implicitly by $|y'(x)| = \Delta y/\Delta x$ or explicitly by $\Delta x = \Delta y/|y'(x)|$. Setting $\langle\hat{M}\rangle \equiv y$ and $\phi \equiv x$ gives Eq. (5.11) for the the minimal detectable phase, $\Delta\phi$, if we identify $\Delta\hat{M} \cong \Delta\langle\hat{M}\rangle$.

Next, we calculate this minimal detectable phase for three different measurement schemes which can be realistically implemented in the laboratory. From now on we take $\alpha_0 = \beta_0$ for simplicity.

5.4.1 Phase sensitivity for the difference counts

We start by analyzing the minimum phase sensitivity for the photon difference counts or photocurrent difference between the photons at the exit ports of the interferometer, i.e. $\hat{M}_1 = \hat{b}_3^\dagger\hat{b}_3 - \hat{a}_3^\dagger\hat{a}_3$. We can get $\langle M_1\rangle$ by simply subtracting the single counts:

$$\langle\hat{a}_3^\dagger\hat{a}_3\rangle = \sinh^2 g + |\alpha_0|^2 A_1\left[1 - \sin(\phi)\right], \tag{5.12}$$

$$\langle \hat{b}_3^\dagger \hat{b}_3 \rangle = \sinh^2 g + |\alpha_0|^2 A_1 \left[1 + \sin(\phi) \right]. \tag{5.13}$$

where

$$A_1 = 1 + 2 \sinh^2 g + \sinh 2g \cos(\psi - 2\theta), \tag{5.14}$$

and θ is the phase of the coherent field α_0. The first term in Eqs. (5.12) and (5.13) is the intensity of spontaneously produced photons. The total number of photons in the stimulated process is given by

$$N_T = 2 \sinh^2 g + 2|\alpha_0|^2 A_1. \tag{5.15}$$

Hence, by using Eqs. (5.12) and (5.4) the difference count signal is found to be

$$\langle \hat{M}_1 \rangle = 2|\alpha_0|^2 A_1 \sin(\phi). \tag{5.16}$$

Note that this signal is zero for spontaneously produced photons. Next, we need to calculate the fluctuations in $\hat{M}_1$ which contains the expectation value of the square of $\hat{M}_1$:

$$\langle \hat{M}_1^2 \rangle = \langle \hat{a}_3^{\dagger 2} \hat{a}_3^2 \rangle + \langle \hat{b}_3^{\dagger 2} \hat{b}_3^2 \rangle + \langle \hat{a}_3^\dagger \hat{a}_3 \rangle + \langle \hat{b}_3^\dagger \hat{b}_3 \rangle - 2 \langle \hat{a}_3^\dagger \hat{b}_3^\dagger \hat{b}_3 \hat{a}_3 \rangle. \tag{5.17}$$

This is a more complicated expression than the signal itself. It contains the two-photon absorptions at the detectors D_a and D_b and the two-photon coincidence counts. Straightforward calculations give the expressions for the first, second and the last term of the Eq. (5.17):

$$\begin{aligned}
\langle \hat{a}_3^{\dagger 2} \hat{a}_3^2 \rangle &= B_2 - \sin(\phi)|\alpha_0|^2 \left\{ 2|\alpha_0|^2 A_1^2 + 4A_1 \sinh^2 g + A_2 \sinh 2g \right\} \\
&+ \sin^2(\phi) \left\{ |\alpha_0|^4 A_1^2 + |\alpha_0|^2 A_2 \sinh 2g + \sinh^2 g(1 + \sinh^2 g) \right\}, \tag{5.18}
\end{aligned}$$

$$\begin{aligned}
\langle \hat{b}_3^{\dagger 2} \hat{b}_3^2 \rangle &= B_2 + \sin(\phi)|\alpha_0|^2 \left\{ 2|\alpha_0|^2 A_1^2 + 4A_1 \sinh^2 g + A_2 \sinh 2g \right\} \\
&+ \sin^2(\phi) \left\{ |\alpha_0|^4 A_1^2 + |\alpha_0|^2 A_2 \sinh 2g + \sinh^2 g(1 + \sinh^2 g) \right\}, \tag{5.19}
\end{aligned}$$

$$\langle \hat{a}_3^\dagger \hat{b}_3^\dagger \hat{b}_3 \hat{a}_3 \rangle = A + B \left[1 + \cos(2\phi) \right], \tag{5.20}$$

where

$$A_2 = \sinh 2g + (1 + 2 \sinh^2 g) \cos(\psi - 2\theta), \tag{5.21}$$

$$B_2 = 2\sinh^4 g + |\alpha_0|^4 A_1^2 + 4|\alpha_0|^2 A_1 \sinh^2 g, \tag{5.22}$$

$$A = \sinh^4 g + 2|\alpha_0|^2 A_1 \sinh^2 g, \tag{5.23}$$

$$B = \frac{1}{2}\left\{\sinh^2 g(1 + \sinh^2 g) + |\alpha_0|^2 A_2 \sinh 2g + |\alpha_0|^4 A_1^2\right\}. \tag{5.24}$$

Then, after a lot of simplification, the variance of the signal $\hat{M}_1$ is found to be

$$(\Delta \hat{M}_1)^2 = 2|\alpha_0|^2 + 4\sin^2(\phi)\left\{|\alpha_0|^2 A_2 \sinh 2g + \sinh^2 g(1 + \sinh^2 g)\right\}. \tag{5.25}$$

Note that the variance is equal to N_T when only coherent fields ($g = 0$) are used, whereas it is equal to N_T^2 when only spontaneously produced photons ($\alpha_0 = 0$) are used. The first term in the curly bracket results from the stimulated process. This term increases the order of fluctuations further to N_T^3 if we assume that the stimulating field's intensity is of the order of spontaneously produced photons, i.e. $|\alpha_0|^2 \sim \sinh^2 g$. Now we are ready to obtain an expression for the minimum phase sensitivity given by Eq. (5.11). Note that with the results given by Eqs. (5.25) and (5.16), this expression depends on the measured phase. Since a zero phase can always be obtained by monitoring a null in the interference pattern, without a loss of generality, we may set $\phi = 0$ to obtain

$$\Delta\phi|_{\phi=0} = \frac{1}{\sqrt{2}|\alpha_0|\left[1 + 2\sinh^2 g + \sinh 2g \cos(\psi - 2\theta)\right]}. \tag{5.26}$$

When the interferometer runs only with classical fields (set $g = 0$), we obtain the usual shot noise sensitivity of $1/\sqrt{N_T}$. However, for the stimulated process, with the assumption $|\alpha_0|^2 \sim \sinh^2 g$, in the high intensity regime, we reach a sensitivity of $\sim 1/N_T^{3/4}$ by surpassing the shot noise limit. We show the plot of this result in Fig. 5.2.

5.4.2 Phase sensitivity for the two-photon coincidence counts and the two-photon absorption

Next, we analyze the minimum sensitivity limit $\Delta\phi$ for the two-photon coincidence signal $\hat{M}_2 = \hat{a}_3^\dagger \hat{b}_3^\dagger \hat{b}_3 \hat{a}_3$ and the two-photon absorption $\hat{M}_3 = \hat{a}_3^{\dagger 2} \hat{a}_3^2$ at the detector D_a

as already given by Eqs. (5.20) and (5.18) respectively. What we need to do next is to calculate the variances for $\hat{M}_2$ and $\hat{M}_3$. Since these calculations are extremely long and complicated to write here, we show the results by plotting the minimum phase sensitivities in Fig. 5.2.
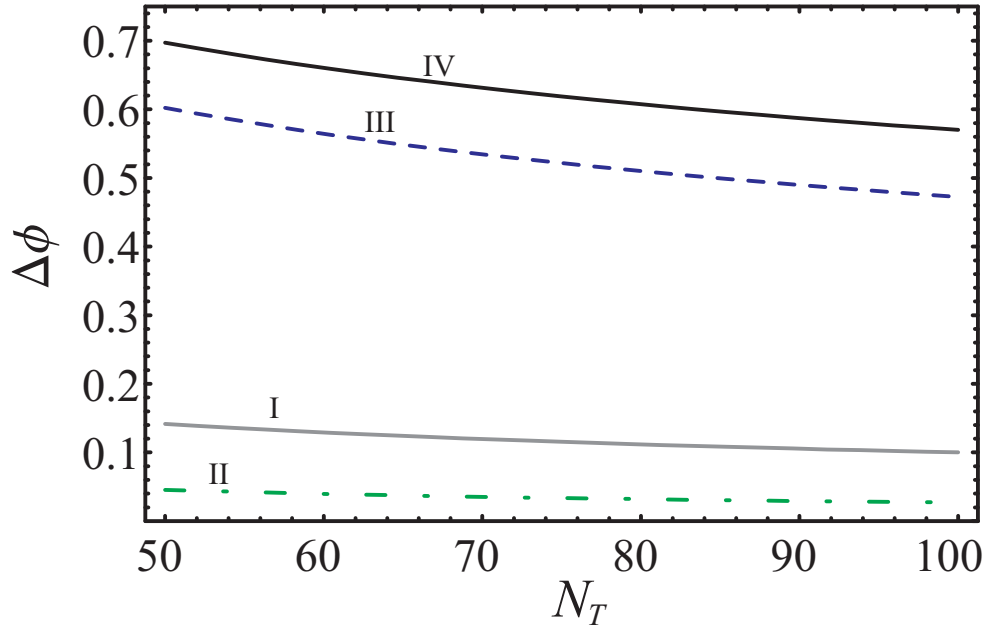
Figure 5.2: Minimum phase sensitivity with respect to total number of photons measured using stimulated parametric down-conversion. The gray line (I) shows the shot noise limit for comparison. The green dotted-dashed line (II), the blue dashed line (III) and the black line (IV) shows the minimum sensitivity for the signals $\hat{M}_1 = \hat{b}_3^\dagger \hat{b}_3 - \hat{a}_3^\dagger \hat{a}_3$, $\hat{M}_2 = \hat{a}_3^\dagger \hat{b}_3^\dagger \hat{b}_3 \hat{a}_3$ and $\hat{M}_3 = \hat{a}_3^{\dagger 2} \hat{a}_3^2$ respectively. The phase uncertainty $\Delta\phi$ is given in radians.

In Fig. 5.2 we show the collective results for the three measurements. We compare the minimum phase uncertainties of these measurements to the case where only coherent fields are used (see Fig. 5.3). For the signal of $\hat{M}_1$ the sensitivity goes below the shot noise level when a stimulated process is used. However, for the signals $\hat{M}_2$ and $\hat{M}_3$ the sensitivities have become somewhat worse when a stimulated down-conversion
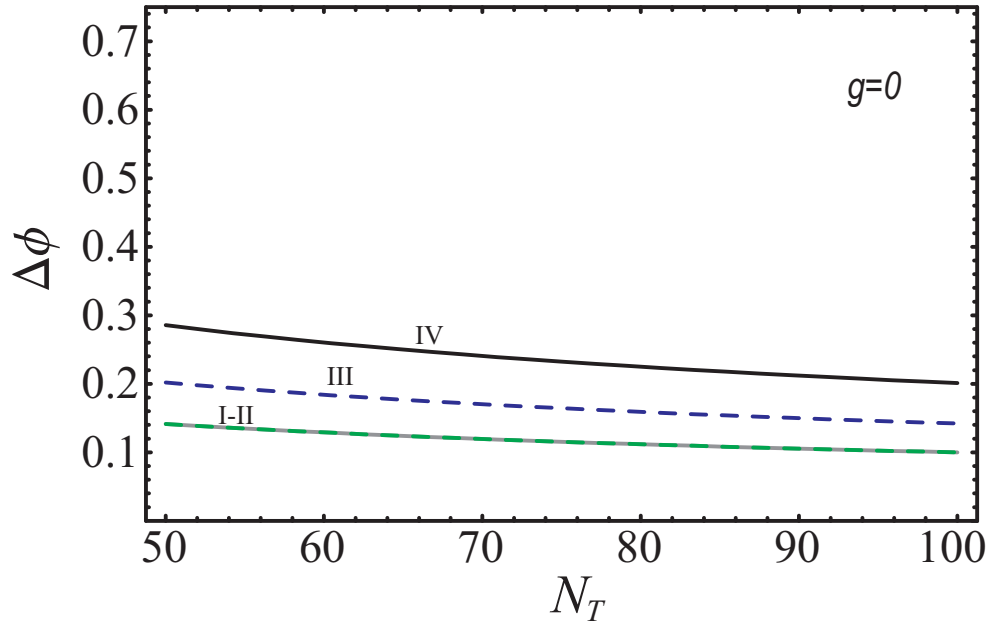
Figure 5.3: The same as in Fig. 5.2 using coherent fields only ($g = 0$).

process is used. In order to reach the full advantage of quantum interferometry, both resolution and sensitivity enhancements are required. This is what we expect from the two-photon coincidence measurement scheme, $\hat{M}_2$. At this point, to understand the differences in the sensitivity calculations for the two regimes (the stimulated process vs. the coherent fields only) further analysis seems to be desired.

CHAPTER 6

SUMMARY AND OUTLOOK

The works of this dissertation were mainly concerned with the following questions:

- How can the images be formed with higher resolution or better sensitivity through the use of quantum states of light?

- How can we beat the Rayleigh resolution or diffraction limit which was caused by the noise properties of the coherent sources of light?

- How can we increase the measurement sensitivity and resolution in interferometry and magnetometry by using entangled photons?

- How are the resolution sensitivity and the measurement strategy related to each other?

In fact, the questions above are closely related to each other in the context of *fundamental limits to measurement* in quantum mechanics. We have identified three specific systems to address these questions. In this concluding chapter we give a brief summary of what we have done and we describe further possibilities to extend these works.

In chapter 2, we have found that the sensitivity of a Sagnac interferometer could be considerably improved by utilizing nonclassical correlations of entangled photons produced by parametric down-conversion. We proposed that by using four single-photon detectors in an unusual unbalanced detection scheme, the resolution sensitivity could be improved by a factor of 4 through photon-photon correlation measurements.

The possibilities for higher order resolution enhancement are open. The unavoidable effect of photon losses inside the interferometer is also a question that needs to be tackled.

It is known that anisotropic properties of a medium can be obtained using magneto-optical rotation (MOR) of linearly polarized coherent light. In chapter 3, we showed that it is possible to improve MOR resolution by a factor of 4 in comparison to coherent light by using polarization entangled photons and a special photon-photon correlation measurement scheme. We investigated the possibility of reaching the Heisenberg limit for the minimum MOR uncertainty in a medium where the anisotropy is induced by an external magnetic field. Hence measuring MOR using entangled photons yields a more precise measurement of the external field. Moreover, one may increase the resolution by increasing the multiple coincidences of photon correlation measurements. This, however, requires multi-photon entangled states with higher intensity. Because the probability of multi-photon entangled states decreases very rapidly at the low gain limit one may have to use stimulated emission of polarized-entangled-photons with multi-pass amplification as in reference [81]. Further research along these lines would be very desirable. It would also be very interesting to adapt these studies to the case where spin-entangled or spin-squeezed atoms are used instead of the entangled photons, to measure the magnetic field since these systems can give more precise results in quantum magnetometry.

In chapter 4, we proposed a new idea using coherent-beam-stimulated parametric processes along with spontaneous ones to produce resolution improvement in an interferometer while at the same time maintaining high visibility at large gains of the parametric process. The results showed that stimulated processes enhance the count rate by several orders of magnitude with a visibility of 100%. Furthermore, we have found that the phases of coherent fields can also be used as tuning knobs to control the visibility of the pattern. In a possible future work, we plan to investigate the ways

of improving the rate of two-photon absorption in quantum lithography. The use of stimulated processes in multi-photon coincidence events is expected to produce even bigger advantages, for example in producing much higher count rates. It is probable that utilizing stimulated processes along with spontaneous ones would change our landscape as far as the fields of imaging and quantum sensors are concerned.

Another point of interest in working with the stimulated parametric process is the minimum phase uncertainty that can reached in the phase measurement. The main objective of quantum interferometry with entangled sources is both to enhance the resolution (super-resolution) and to decrease the measured phase uncertainty (super-sensitivity). Even though the resolution enhancement is possible by the use of coherent sources [82], nonclassical sources of light are needed to obtain increased phase accuracy. Therefore, in chapter 5, we analyzed the minimum phase uncertainty of the Mach-Zehnder interferometer with stimulated parametric down-conversion input. We showed that it is possible to decrease the phase uncertainty below the shot noise level for the measurement of photon difference at the output ports. We also analyzed the minimum phase sensitivity for the two-photon coincidence counting and the two-photon absorption signal. We think that further analysis of different measurement schemes would be required to reach both the super-resolution and the super-sensitivity.

BIBLIOGRAPHY

[1] A. N. Boto, P. Kok, D. S. Abrams, S. L. Braunstein, C. P. Williams, and J. P. Dowling, "Quantum interferometric optical lithography: Exploiting entanglement to beat the diffraction limit," Phys. Rev. Lett. **85,** 2733–2736 (2000).

[2] M. D'Angelo, M. V. Chekhova, and Y. Shih, "Two-photon diffraction and quantum lithography," Phys. Rev. Lett. **87,** 013602 (2001).

[3] S. J. Bentley, and R. W. Boyd, "Nonlinear optical lithography with ultra-high sub-Rayleigh resolution," Optics Express **12**, 5735 (2004).

[4] V. Giovannetti, S. Lloyd and L. Maccone, "Quantum-enhanced measurements: Beating the standard quantum limit," Science **306**, 1330 (2004).

[5] Z. Y. Ou, "Complementarity and fundamental limit in precision phase measurement," Phys. Rev. Lett. **77**, 2352 (1996).

[6] V. Giovannetti, S. Lloyd and L. Maccone, "The role of entanglement in dynamical evolution," Europhys. Lett. **62**, 615 (2004).

[7] P. Kwiat, H. Weinfurter, T. Herzog, A. Zeilinger, and Mark A. Kasevich, "Interaction-Free Measurement," Phys. Rev. Lett. **74**, 4763–4766 (1995).

[8] P. G. Kwiat, A. G. White, J. R. Mitchell, O. Nairz, G. Weihs, H. Weinfurter, and A. Zeilinger, "High-Efficiency Quantum Interrogation Measurements via the Quantum Zeno Effect," Phys. Rev. Lett. **83**, 4725–4728 (1999).

[9] T. B. Pittman, Y. H. Shih, D. V. Strekalov, and A. V. Sergienko, "Optical imaging by means of 2-photon quantum entanglement," Phys. Rev. A **52,** R3429–R3432 (1995).

[10] C. K. Hong, Z. Y. Ou, and L. Mandel, "Measurement of subpicosecond time intervals between two photons by interference," Phys. Rev. Lett. **59**, 2044–2046 (1987).

[11] Y. H. Shih, A. V. Sergienko, M. H. Rubin, T. E. Kiess, and C. O. Alley, "Two-photon interference in a standard Mach-Zehnder interferometer," Phys. Rev. A **49**, 4243 (1994).

[12] Z. Y. Ou, X. Y. Zou, L. J. Wang, and L. Mandel, "Experiment on nonclassical 4th-order interference," Phys. Rev. A **42,** 2957–2965 (1990).

[13] J. G. Rarity, P. R. Tapster, E. Jakeman, T. Larchuk, R. A. Campos, M. C. Teich, and B. E. A. Saleh, "2-photon interference in a mach-zehnder interferometer," Phys. Rev. Lett. **65,** 1348–1351 (1990).

[14] P. G. Kwiat, K. Mattle, H. Weinfurter, A. Zeilinger, A. V. Sergienko, and Y. Shih, "New High-Intensity Source of Polarization-Entangled Photon Pairs," Phys. Rev. Lett. **75**, 4337 (1995).

[15] S. Friberg, C.K. Hong and L. Mandel, "Measurement of Time Delays in the Parametric Production of Photon Pairs," Phys. Rev. Lett. **54**, 2011 (1985).

[16] L. Mandel and E. Wolf, Chaps. 12 and 22 in *Coherence and Quantum Optics* (Cambridge University Press, Cambridge, England, 1995).

[17] C. M. Caves, "Quantum-mechanical noise in an interferometer," Phys. Rev. D **23,** 1693–1708 (1981).

[18] Yurke B, McCall S L, and Klauder J R, "SU(2) and SU(1,1) interferometers," Phys. Rev. A **33,** 4033–4054 (1986).

[19] J. P. Dowling, "Correlated input-port, matter-wave interferometer: Quantum-noise limits to the atom-laser gyroscope," Phys. Rev. A **57,** 4736-4746 (1998).

[20] M. J. Holland and K. Burnett, "Interferometric detection of optical-phase shifts at the heisenberg limit," Phys. Rev. Lett. **71,** 1355–1358 (1993).

[21] A. F. Abouraddy, B. E. A. Saleh, A. V. Sergienko, and M. C. Teich, " Role of entanglement in two-photon imaging ," Phys. Rev. Lett. **87,** 123602 (2001).

[22] G. S. Agarwal, R. W. Boyd, E. M. Nagasako, and S. J. Bentley, "Comment on "Quantum interferometric optical lithography: Exploiting entanglement to beat the diffraction limit"," Phys. Rev. Lett. **86,** 1389–1389 (2001).

[23] G. Björk, L. L. Sanchez-Soto, and J. Söderholm, "Entangled-state lithography: Tailoring any pattern with a single state," Phys. Rev. Lett. **86,** 4516–4519 (2001).

[24] G. S. Agarwal and M. O. Scully, "Magneto-optical spectroscopy with entangled photons," Opt. Lett. **28,** 462–464 (2003).

[25] E. Schrödinger, "Die gegenwärtige Situation in der Quantenmechanik," Naturwissenschaften **23**, 807-812 (1935).

[26] A. Einstein, B. Podolsky, and N. Rosen, "Can quantum mechanical description of physical reality be considered complete?," Phys. Rev. **47**, 777-779, (1935).

[27] H. Lee, P. Kok, and J. P. Dowling, "A quantum Rosetta stone for interferometry," J. Mod. Opt. 49, 2325–2338 (2002).

[28] G. Sagnac, "L'éther lumineux démontré par l'effect du vent relatif d'éther dans un interféromètre en rotation uniforme," C. R. Acad. Sci. **157,** 708–710 (1913).

[29] G. Bertocchi, O. Alibart, D. B. Ostrowsky, S. Tanzilli, and P. Baldi, "Single-photon Sagnac interferometer," J. Phys. B **39,** 1011–1016 (2006).

[30] P. Grangier, G. Roger, and A. Aspect, "Experimental evidence for a photon anticorrelation effect on a beam splitter: a new light on single-photon interferences," Europhys. Lett. **1,** 173 (1986).

[31] P. Hariharan, N. Brown, and B. C. Sanders, "Interference of independent laser-beams at the single-photon level," J. Mod. Opt. **40,** 113–122 (1993).

[32] A. Zeilinger, "Experiment and the foundations of quantum physics," Rev. Mod. Phys. **71,** S288–S297 (1999).

[33] E. Yablonovitch and R. B. Vrijen, "Optical projection lithography at half the Rayleigh resolution limit by two-photon exposure," Opt. Eng. **38**, 334–338 (1999).

[34] D. V. Korobkin and E. Yablonovitch, "Two-fold spatial resolution enhancement by two-photon exposure of photographic film," Opt. Eng. **41**, 1729–1732 (2002).

[35] Z. Y. Ou, L. J. Wang, X. Y. Zou, and L. Mandel, "Evidence for phase memory in 2-photon down conversion through entanglement with the vacuum," Phys. Rev. A **41,** 566–568 (1990).

[36] K. Edamatsu, R. Shimizu, and T. Itoh, "Measurement of the photonic de Broglie wavelength of entangled photon pairs generated by spontaneous parametric down-conversion," Phys. Rev. Lett. **89,** 213601 (2002).

[37] M. Eibl, S. Gaertner, M. Bourennane, C. Kurtsiefer, M. Zukowski, and H. Weinfurter, "Experimental observation of four-photon entanglement from parametric down-conversion," Phys. Rev. Lett. **90,** 200403 (2003).

[38] P. Walther, J. W. Pan, M. Aspelmeyer, R. Ursin, S. Gasparoni, and A. Zeilinger, "De Broglie wavelength of a non-local four-photon state," Nature (London) **429,** 158–161 (2004).

[39] J. Jacobson, G. Björk, I. Chuang, and Y. Yamomoto, "Photonic de broglie waves," Phys. Rev. Lett. **74,** 4835–4838 (1995).

[40] O. Steuernagel, "de Broglie wavelength reduction for multiphoton wave packet," Phys. Rev. A **65,** 033820 (2002).

[41] X. Li, P. L. Voss, J. E. Sharping, and P. Kumar, "Optical-fiber source of polarization-entangled photons in the 1550 nm telecom band," Phys. Rev. Lett. **94,** 053601 (2005).

[42] W. Schleich and M. O. Scully 1984 *Modern Trends in Atomic and Molecular Physics, Proceedings of Les Houches Summer School, Session XXXVIII*, edited by R. Stora and G. Grynberg, North Holland, Amsterdam

[43] E. J. Post, "Sagnac effect," Rev. Mod. Phys. **39,** 475 (1967).

[44] F. Jacobs and R. Zamoni, "Laser ring gyro of arbitrary shape and rotation axis," Am. J. Phys. **50,** 659–660 (1982).

[45] M. A. Nielsen and I. L. Chuang, *Quantum computation and quantum information*, (Cambridge University Press, Cambridge, 2000).

[46] C. H. Bennett, D. P. DiVincenzo, J. A. Smolin, and W. K. Wooters, "Mixed-state entanglement and quantum error correction," Phys. Rev. A **54,** 3824–3851 (1996).

[47] M. Caminati, F. De Martini, R. Perris, F. Sciarrino, and V. Secondi, "Nonseparable Werner states in spontaneous parametric down-conversion," Phys. Rev. A **73,** 032312 (2006).

[48] A. Ourjoumtsev, R. Tualle-Brouri, and P. Grangier, "Quantum homodyne tomography of a two-photon fock state ," Phys. Rev. Lett. **96,** 213601 (2006).

[49] G. S. Agarwal, K. W. Chan, R. W. Boyd, H. Cable, and J. P. Dowling "Quantum states of light produced by a high-gain optical parametric amplifier for use in quantum lithography," J. Opt. Soc. Am. B **24,** 270 (2007).

[50] H. J. Chang, H. Shin, M. N. O'Sullivan-Hale, and R. W. Boyd, "Implementation of subRayleigh lithography using an N-photon absorber," J. Mod. Opt. **53,** 2271-2277 (2006).

[51] H. Lefevre, *The Fiber-Optic Gyroscope*, (Artech House, Boston, 1993).

[52] Z.Y. Ou, "Fundamental quantum limit in precision phase measurement," Phys. Rev. A **55**, 2598–2609 (1997).

[53] P. Kok and S.L. Braunstein, "Postselected versus nonpostselected quantum teleportation using parametric down-conversion," Phys. Rev. A **61**, 042304 (2000).

[54] B. Julsgaard, A. Kozhekin and E. S. Polzik, "Experimental long-lived entanglement of two macroscopic objects," Nature (London) **413**, 400 (2001).

[55] B. Yurke, "Input States for Enhancement of Fermion Interferometer Sensitivity," Phys. Rev. Lett. **56**, 1515 (1986).

[56] G. S. Agarwal, and R. R. Puri, "Atomic states with spectroscopic squeezing," Phys. Rev. A **49**, 4968 (1994).

[57] D. J. Wineland, J. J. Bollinger, W. M. Itano, F. L. Moore, and D. J. Heinzen, "Spin squeezing and reduced quantum noise in spectroscopy ," Phys. Rev. A **46**, R6797 (1992).

[58] H. S. Eisenberg, G. Khoury, G. Durkin, C. Simon and D. Bouwmeester, "Quantum Entanglement of a Large Number of Photons," Phys. Rev. Lett. **93**, 193901 (2004).

[59] Kishore T. Kapale, and J. P. Dowling, "Bootstrapping Approach for Generating Maximally Path-Entangled Photon States," Phys. Rev. Lett. **99**, 053602 (2007).

[60] H. Lee, P. Kok, N.J. Cerf and J.P. Dowling, "Linear optics and projective measurements alone suffice to create large-photon-number path entanglement," Phys. Rev. A **65**, 030101(R) (2002).

[61] G. S. Agarwal, K. W. Chan, R. W. Boyd, H. Cable, and J. P. Dowling "Quantum states of light produced by a high-gain optical parametric amplifier for use in quantum lithography," J. Opt. Soc. Am. B **24,** 270 (2007).

[62] B. H. Liu, F. W. Sun, Y. X. Gong, Y. F. Huang, G. C. Guo, and Z. Y. Ou, "Four-photon interference with asymmetric beam splitters," Opt. Lett. **32**, 1320 (2007).

[63] M.W. Mitchell, J.S. Lundeen and A.M. Steinberg, "Super-resolving phase measurements with a multiphoton entangled state," Nature (London) **429**, 161 (2004).

[64] T. Nagata, R. Okamoto, J. L. O'Brien, K. Sasaki, and S. Takeuchi, "Beating the Standard Quantum Limit with Four-Entangled Photons," Science **316**,726-729 (2007).

[65] Aziz Kolkiran, and G. S. Agarwal, "Heisenberg limited Sagnac interferometry," Opt. Express **15**, 6798-6808 (2007).

[66] Aziz Kolkiran, and G. S. Agarwal, "Towards the Heisenberg limit in magnetometry with parametric down-converted photons," Phys. Rev. A **74**, 053810 (2006).

[67] O. Glöckl, U.L. Andersen, and G. Leuchs, "Quantum interferometry," in *Lectures in quantum information* (Wiley-VCH Verlag GmbH & Co KGaA, Weinheim, 2006), pp. 575-590.

[68] A. Gatti, E. Brambilla, and L. A. Lugiato, "Entangled Imaging and Wave-Particle Duality: From the Microscopic to the Macroscopic Realm," Phys. Rev. Lett. **90**, 133603 (2003).

[69] Baris I. Erkmen, and Jeffrey H. Shapiro, "Ghost Imaging: What is quantum, what is not," http://arxiv.org/abs/quant-ph/0612070.

[70] R. S. Bennink, S. J. Bentley, R. W. Boyd, and J. C.Howell, "Quantum and Classical Coincidence Imaging," Phys. Rev. Lett. **92**, 033601 (2004).

[71] P. H. Souto Ribeiro, and G. A. Barbosa, "Direct and ghost interference in double-slit experiments with coincidence measurements," Phys. Rev. A **54**, 3489 (1996).

[72] F. Sciarrino, C. Vitelli, F. De Martini, R. G. Glasser, H. Cable, and J. P. Dowling, "Experimental sub-Rayleigh resolution by an unseeded high-gain optical parametric amplifier for quantum lithography," Phys. Rev. A **77**, 012324 (2008).

[73] K. S. Thorne, "Gravitational-wave research: Current status and future prospects," Rev. Mod. Phys. **52**, 285 - 297 (1980).

[74] "Quantum Optics, Experimental Gravitation and Measurement Theory," edited by P. Meystre and M. O. Scully (Plenum, New York, 1983).

[75] J. Gea-Banacloche and G. Leuchs, "Squeezed States for Interferometric Gravitational-wave Detectors ," J. Mod. Opt. **34**, 793 (1987).

[76] R. S. Bondurant, and J. H. Shapiro, "Squeezed states in phase-sensing interferometers," Phys. Rev. D **30**, 2548 (1984).

[77] P. Grangier, R. E. Slusher, B. Yurke, and A. LaPorta, "Squeezed-lightenhanced polarization interferometer," Phys. Rev. Lett. **59**, 2153 (1987).

[78] M. Xiao, L.-A. Wu, and H. J. Kimble, "Precision measurement beyond the shot-noise limit," Phys. Rev. Lett. **59**, 278 (1987).

[79] P. A. M. Dirac, "The Quantum Theory of the Emission and Absorption of Radiation," Proc. R. Soc. London Ser. A **114**, 243 (1927)

[80] W. Heitler, "The Quantum Theory of Radiation," 3rd ed. (Oxford University Press, London, 1954), p. 65.

[81] A. Lamas-Linares, J. C. Howell, and D. Bouwmeester, "Stimulated emission of polarization-entangled photons," Nature (London) **412**, 887 (2001).

[82] K. J. Resch, K. L. Pregnell, R. Prevedel, A. Gilchrist, G. J. Pryde, J. L. O'Brien, and A. G. White, "Time-Reversal and Super-Resolving Phase Measurements," Phys. Rev. Lett. **98**, 223601 (2007).

APPENDIX A

FOUR-PHOTON PROBABILITY

In this appendix we show the details of the calculation leading to the result given in Eq. (3.17). One can obtain the result first by solving the Schrödinger equation for the state $|1_{\hat{a}_H} 1_{\hat{a}_V} 1_{\hat{b}_H} 1_{\hat{b}_V}\rangle$ in the four-photon subspace of the electromagnetic field and having the inner product with the state $|\psi_{non}\rangle$. Since the parts of the Hamiltonian having $\hat{a}$ and $\hat{b}$ modes commute, we can solve the Schrödinger equation for the states $|1_{\hat{a}_H} 1_{\hat{a}_V}\rangle$ and $|1_{\hat{b}_H} 1_{\hat{b}_V}\rangle$ separately. Let us start with a general time-dependent state in the $\hat{a}_H$ and $\hat{a}_V$ modes which contains two photons totally;

$$|\psi(t)\rangle = c(t)|20\rangle + d(t)|02\rangle + f(t)|11\rangle \tag{A.1}$$

with the initial condition $|\psi(0)\rangle = |11\rangle$. Solving the Schrödinger equation by using the effective Hamiltonian $H = \chi_+ \hat{a}_+^\dagger \hat{a}_+ + \chi_- \hat{a}_-^\dagger \hat{a}_-$ gives us the result

$$
\begin{aligned}
|\psi(t)\rangle &= e^{-it\chi}[\frac{1}{\sqrt{2}} \sin(\Omega t)|20\rangle - \frac{1}{\sqrt{2}} \sin(\Omega t)|02\rangle \\
&+ \cos(\Omega t)|11\rangle]
\end{aligned}
\tag{A.2}
$$

where $\chi = \chi_+ + \chi_-$ and $\Omega = \chi_+ - \chi_-$. For a medium of length l, the angle Ωt corresponds to the MOR angle ϕ which is given in Eq. (3.5). The solution for the state $|1_{\hat{b}_H} 1_{\hat{b}_V}\rangle$ can be obtained just by replacing ϕ by $-\phi$ because the direction of propagation of the $\hat{b}$ modes are opposite to that of $\hat{a}$ modes inside the medium. This is the reason that the part of the effective Hamiltonian for the $\hat{b}_\pm$ modes takes a minus sign in Eq. (3.15). Consequently we can write the solution of the Schrödinger equation for the state $|1_{\hat{a}_H} 1_{\hat{a}_V} 1_{\hat{b}_H} 1_{\hat{b}_V}\rangle$ as:

$$\exp(-itH_{med})|1_{\hat{a}_H} 1_{\hat{a}_V} 1_{\hat{b}_H} 1_{\hat{b}_V}\rangle = e^{-it\chi} \left[\frac{1}{\sqrt{2}} \sin\phi |20\rangle - \frac{1}{\sqrt{2}} \sin\phi |02\rangle + \cos\phi |11\rangle \right]$$

$$\otimes \quad e^{-it\chi} \left[-\frac{1}{\sqrt{2}} \sin\phi |20\rangle + \frac{1}{\sqrt{2}} \sin\phi |02\rangle + \cos\phi |11\rangle \right].$$

$$(A.3)$$

Taking the inner product of this with the state $|\psi_{non}\rangle$ and having the absolute square gives us the result given in Eq. (3.17).

The result given in Eq. (3.18) can be obtained by following the same method given above.

VITA

Aziz Kolkıran

Candidate for the Degree of

Doctor of Philosophy

Dissertation: QUANTUM IMAGING AND SENSING WITH ENTANGLED PHO-
TONS

Major Field: Photonics

Biographical:

Personal Data: Born in Izmir, Turkey on June 20, 1973.

Education:
Received the B.S. degree from Middle East Technical University, Ankara,
Turkey, 1996, in Physics.
Received the B.S. degree from Middle East Technical University, Ankara,
Turkey, 1996, in Mathematics.
Received the M.S. degree from Middle East Technical University, Ankara,
Turkey, 1999, in Physics.
Completed the requirements for the degree of Doctor of Philosophy with a
major in Photonics from Oklahoma State University in May, 2008.

Name: Aziz Kolkiran   Date of Degree: July, 2008

Institution: Oklahoma State University   Location: Stillwater, Oklahoma

Title of Study: QUANTUM IMAGING AND SENSING WITH ENTANGLED
PHOTONS

Pages in Study: 66   Candidate for the Degree of Doctor of Philosophy

Major Field: Photonics

This dissertation contains new theoretical work on how to utilize the entangled photons produced in a parametric down conversion to improve resolution and sensitivity in quantum interferometry, magnetometry and lithography. Chapter 1 introduces some basics of quantum imaging and sensing systems and gives an outline of the thesis. Chapter 2 deals with the use of entangled photons in Sagnac interferometry. We introduce the Sagnac ring interferometer and analyze the Sagnac phase shift with classical and quantum inputs of light. We compare the results obtained from entangled photon pairs input with classical and single-photon inputs. We show how the photon-photon correlation measurements increase the resolution and the sensitivity in the phase shift. In chapter three, we present an analysis of how parametric down-converted photons could be utilized in getting better spectroscopic information about a medium which has magnetic field induced anisotropy. We demonstrate how the improvement in magneto-optical rotation (MOR) of light could be realized by employing two different schemes with collinear and noncollinear down-conversion geometries compared to the use of coherent light. We calculate the resolution that can be achieved in the MOR's both by the use of coherent light and down-converted light. We discuss the possibility that the Heisenberg limit could be reached in magnetometry by the use of down-converted light. In chapter 4, we propose a new idea of using coherent beam stimulated parametric processes along with spontaneous ones to produce resolution improvement in two-photon interferometry. The stimulated processes enhance the count rate by several orders of magnitude while at the same time maintaining high visibility at large gains of the parametric process. We further find that the phases of coherent fields can also be used as tuning knobs to control the visibility of the pattern. We use coherent beams at the signal and idler frequencies as the seed light for the down-conversion process. In chapter 5, we analyze the minimum phase uncertainty of the phase measurement in a Mach-Zehnder interferometer using stimulated parametric down-conversion. We calculate the phase sensitivities for different measurement schemes. We conclude the thesis in chapter 6 and give an outlook for future work.

ADVISOR'S APPROVAL: ─────────────────────────────────────